Naval Research Laboratory
Washington, DC 20375-5320

NRL/MR/6180--02-8630

The Burning of a Thermoplastic Material Under a Forced-Flow Boundary Layer Flame

CHUKA C. NDUBIZU

GEO-CENTERS, Inc.
Lanham

RAMAGOPAL ANANTH
PATRICIA A. TATEM

Navy Technology Center for Safety and Survivability
Chemistry Division

July 31, 2002

REPORT DOCUMENTATION PAGE

Form Approved
OMB No. 0704-0188

1. REPORT DATE *(DD-MM-YYYY)*	2. REPORT TYPE	3. DATES COVERED *(From - To)*
July 31, 2002	Memorandum Report	October 1, 1999-1 June 2002

4. TITLE AND SUBTITLE

The Burning of a Thermoplastic Material Under a Forced-Flow Boundary Layer Flame

5a. CONTRACT NUMBER

5b. GRANT NUMBER

5c. PROGRAM ELEMENT NUMBER
6213N

6. AUTHOR(S)

Chuka C. Ndubizu,* Ramagopal Ananth, and Patricia A. Tatem

5d. PROJECT NUMBER
MA-123-001-6001

5e. TASK NUMBER
MA-123-001-6001

5f. WORK UNIT NUMBER
MA-123-001-6001

7. PERFORMING ORGANIZATION NAME(S) AND ADDRESS(ES)

Naval Research Laboratory, Code 6180
4555 Overlook Avenue
Washington, DC 20375-5320

8. PERFORMING ORGANIZATION REPORT NUMBER

NRL/MR/6180--02-8630

9. SPONSORING / MONITORING AGENCY NAME(S) AND ADDRESS(ES)

Office of Naval Research
800 North Quincy Street
Arlington, VA 22217-5000

10. SPONSOR / MONITOR'S ACRONYM(S)

11. SPONSOR / MONITOR'S REPORT NUMBER(S)

12. DISTRIBUTION / AVAILABILITY STATEMENT

Approved for public release; distribution is unlimited.

13. SUPPLEMENTARY NOTES

*GEO-CENTERS, Inc., Lanham, MD

14. ABSTRACT

This report presents experimental results of the characterization of forced flow boundary layer burning of poly(methyl methacrylate) (PMMA) without water mist. Small samples (7.5 × 9.5 × 2.5 cm) of black PMMA were burnt at the exit of a wind tunnel at free stream velocities between 60 and 168 cm/s, in tests lasting between 2.5 min and 20 minutes. The results of the gas phase temperature mapping indicate that a stable flame is formed over the sample within a short time after ignition.

The local surface regression rate is transient, decreasing with time near the leading edge and increasing with time downstream. For $60 \leq U_{\infty} \leq 168$ cm/s, the time averaged regression rate in the leading section decreased by about a factor of two between 5 and 20-minute tests. The transient burning rate in the leading section is due to the presence of a valley formed in this section as a result of non-uniform surface regression. On the other hand, the transient regression rate in the trailing section seems to be due mainly to in-depth solid heat conduction.

15. SUBJECT TERMS

Boundary layer burning, PMMA, Water mist, Forced flow, Temperature mapping

16. SECURITY CLASSIFICATION OF:			17. LIMITATION OF ABSTRACT	18. NUMBER OF PAGES	19a. NAME OF RESPONSIBLE PERSON
a. REPORT	b. ABSTRACT	c. THIS PAGE			Dr. Ramagopal Ananth
Unclassified	Unclassified	Unclassified	UL	50	19b. TELEPHONE NUMBER *(include area code)* (202) 767-3197

Standard Form 298 (Rev. 8-98)
Prescribed by ANSI Std. Z39.18

CONTENTS

The Burning of a Thermoplastic Material Under a Forced-Flow Boundary Layer Flame.

1.0 INTRODUCTION

Boundary layer type diffusion flames have been widely studied because of their importance in wall fires, ceiling fires, and wind-driven fires on flat surfaces such as roofs and floors. Bulkhead fires and spilled fuel fires on aircraft carrier decks are typical examples of boundary layer type fires in the Navy. In order to effectively control these fires, there is need to understand the stability, flame spread mechanisms, suppression and extinction mechanisms in boundary layer type fires. To study these phenomena it is often desirable to characterize a stable unsuppressed flame to begin with before conditions are changed to obtain instability or suppression. Our eventual goal is to study the controlling mechanisms for the suppression of boundary layer-type fires using water mist. Therefore, a detailed characterization of the burning sample without mist is desirable so as to establish the base case conditions. This report presents the results of experiments to establish the base case conditions in boundary layer combustion of poly(methyl methacrylate) (PMMA). PMMA burns clean and hence it has been widely used in laboratory experiments to study various fire phenomena.

The combustion of solid and liquid fuels is characterized by a complex coupling of chemical reactions and transport processes in the condensed and the gas phases, as well as the coupling of these processes between the two phases. For example, combustion in the gas phase generates heat, which is fed back to the condensed material to produce gaseous fuel on which the combustion reactions depend. The suppression of fire over a solid material depends on the effects of the suppressant on these coupled processes. The gasification of the solid and char formation are some of the complex solid phase processes, which depend on heat feedback as well as affect the burning rate. These processes need to be understood in order to address effectively the suppression problem. In PMMA combustion, heat fed back from the flame softens the surface to form a melt layer, which pyrolyzes, producing mainly methyl methacrylate monomer [1]. Since PMMA pyrolysis leaves no char, the sample surface level regresses as the gaseous products leave the surface. In boundary layer combustion of a condensed fuel the heat feedback to the fuel surface is very high in the leading section where the flame is closest to the surface and decreases with the stream-wise distance. Consequently, the PMMA burning rate will vary with stream-wise distance and this will be quantified in the report.

This report will present gas phase and melt layer temperatures as well as surface regression rate data and use them to discuss the coupling of the gas phase and solid phase processes for the base case (no suppressant). A similar study was carried out by Krishnamurthy and Williams [2], who measured PMMA regression rate in non-spreading boundary layer diffusion flames. They investigated the relationship between the regression rate and surface temperature since they were interested in determining the chemical kinetic parameters for PMMA pyrolysis. They also experimentally verified of the classical Emmons's model [3] of laminar forced flow boundary layer flame for calculating the surface regression rate of PMMA within a short time (30 seconds) after ignition. In a related study, Hirano et al. [4] studied the burning of methanol and ethanol in a forced flow boundary layer configuration. They studied the

Manuscript approved July 2, 2002.

coupling between gas phase and solid phase processes. They showed from numerical predictions and experimental data that the burning rate increased with free stream velocity as a result of increased heat convection to the condensed fuel.

Agrawal [5] studied the burning of a 30 cm PMMA sample during wind-aided flame spread. They measured the sample surface regression rate and related that to the heat flux to the PMMA surface at high wind velocities (>1.0 m/s). In a similar study Atreya and Mekki [6] measured the heat feedback to a flat plate surface over which a methane boundary layer flame was burning and showed that the heat feedback to the flat surface varies as $X^{-0.5}$ underneath the flame as predicted by the classical theory, but varies as $X^{-2.8}$ beyond the flame tip. PMMA has been used extensively to study flame spread over solid fuels and Fernandez-Pello and Hirano [7] published a comprehensive review of these studies. In most flame spread studies in the literature, the spread rate is much higher than the PMMA surface regression rate. However, this report focuses on tests where the spread rate is either zero or is much less than the regression rate.

Since PMMA is used extensively in solid fuel combustion studies, it is essential to understand the gasification characteristics of PMMA and this was addressed by Kashiwagi and co-workers [e.g., 8,9], who studied the gasification of PMMA under flaming and non-flaming conditions. They showed that PMMA does not vaporize at a constant temperature and that the pyrolyzing surface temperature tends to increase with heat flux input to the surface [8]. In non-flaming gasification of PMMA they showed that increased oxygen concentration in the surrounding air enhances bubbling and solid gasification. It was reported [9] that increased oxygen concentration increases the pyrolyzing surface temperature. This lowers the viscosity of the melt near the surface and makes it easier for bubbles to escape. Vovelle et al. [10] and Tewarson and Pion [11] studied the effects of sample thickness on the burning rate. They showed that heat transfer through the back of a PMMA sample becomes significant when the sample thickness decreases below 1.5 cm and thereafter the burning rate is a function of sample thickness.

This work is a prelude to the study of water mist suppression of boundary layer flames. The key objective of this work is to fully characterize laminar boundary layer combustion of a PMMA sample without suppressant. The coupling of the gas phase and solid phase processes will be addressed. In particular, the effects of non-uniform surface regression rate on the local burning rate and flame stability, as well as the implications of these effects on suppression effectiveness, will be discussed in detail.

2.0 EXPERIMENTAL

Figure 1 shows a schematic of the experimental setup. It consists of the wind tunnel, the PMMA sample and the sample holder, an ATC® weigh platform, thermocouples mounted on a set of Velmex X-Y unislides. The wind tunnel has a 36 X 45 X 61 cm plenum at one end into which an Ametek RJ054 ® variable speed blower pumps air. Pressure build up in the plenum drives the flow of the oxidizer through the wind tunnel and hence the effects of the blower on the flow are minimized. The flow velocity in the wind tunnel is selected by adjusting the speed of the blower. The burning sample is positioned outside the tunnel, at the center of the tunnel exit.

This makes it easier for the thermocouples to be moved freely in and out of the flame to measure the gas phase temperatures.

The sample holder is made of a 1.5-mm-thick aluminum plate (18.5 cm x 19 cm) brazed onto a 10 cm x 8 cm x 2.1 cm deep cup, which holds the PMMA sample. This provides a 4-cm lip in the leading section and a 5-cm lip in the other three sides. At the measurement location, the holder is positioned with its leading edge against the tunnel exit at the center of the channel (see insert in Fig.1). A thin strip of quartz glass is placed between the PMMA sample and the walls of the holder on all the four sides to prevent molten PMMA from sticking on the walls of the sample holder. The sample holder sits on a platform mounted on a slide mechanism such that the sample can be ignited under the radiant panel located about 50 cm downstream from the tunnel exit and quickly moved to the tunnel exit after ignition.

Five R-type thermocouples, 50 μm (0.002") in diameter, are mounted on the X-Y unislide arrangement such that they can be moved precisely up and down (Y- direction) across the flame thickness or left and right (X-direction) along the length of the flame. Voltage signal from the thermocouples go through National Instruments ® TC 2095 terminal block into the SCXI 2000 chassis where the signals are conditioned and digitized. LabView software is used to precisely position the thermocouples as well as read the digitized signals and to convert them to temperatures. A picture of the actual experimental setup is shown in Fig. 2.

2.1 Test Procedure

The 7.5 x 9.5 cm PMMA samples are made from Cyro ® Acrylite GP sheet nominally 2.54 cm thick. The choice of sample thickness is influenced by the work of Vovelle et al. [10] and also Tewarson and Pion [11], which showed that the initial sample thickness does not affect the burning rate if it is larger than 1.5 cm. The inlet velocity (U) of the air at the exit of the tunnel (measurement location) is measured using a hot wire anemometer. The velocity profile across the tunnel is not fully developed and it is relatively uniform near the center. The uniform velocity near the center of the tunnel is the free stream velocity U_∞.

The entire sample surface is ignited by exposure to a uniform irradiation from a radiant panel. The process of irradiation, surface gasification and the establishment of a stable 2-D flame over the sample take place in about 40 seconds. Time is started immediately after ignition. Thereafter, the burning sample is quickly moved to the measurement location at the tunnel exit. Gas phase temperatures are measured simultaneously at five X locations with five thermocouples and the measurement is completed within 1 minute. The sample is allowed to burn for a known time interval before the flame is extinguished. After the sample cools down, its thickness along the centerline is measured at various X locations with a digital micrometer whose accuracy is ±0.003 mm. Since the initial thickness of the sample was measured, the sample regression rate at each location is obtained as the difference in thickness, after correction for PMMA thermal expansion, divided by the test duration.

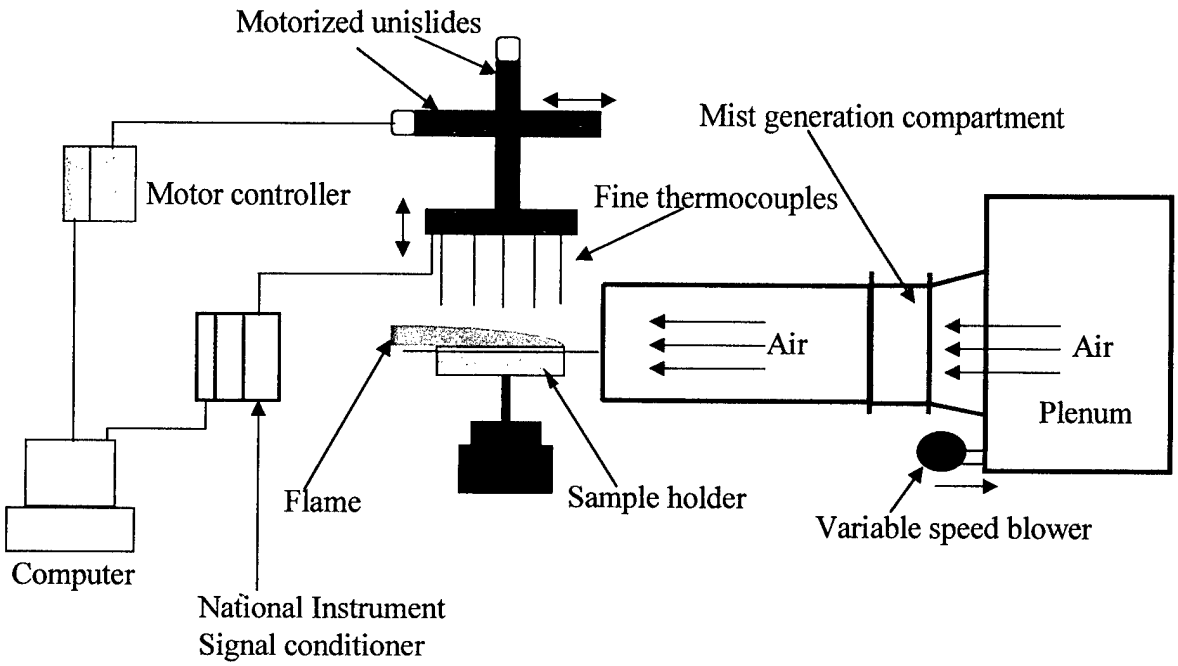

Figure 1: A Schematic of the Experimental Setup

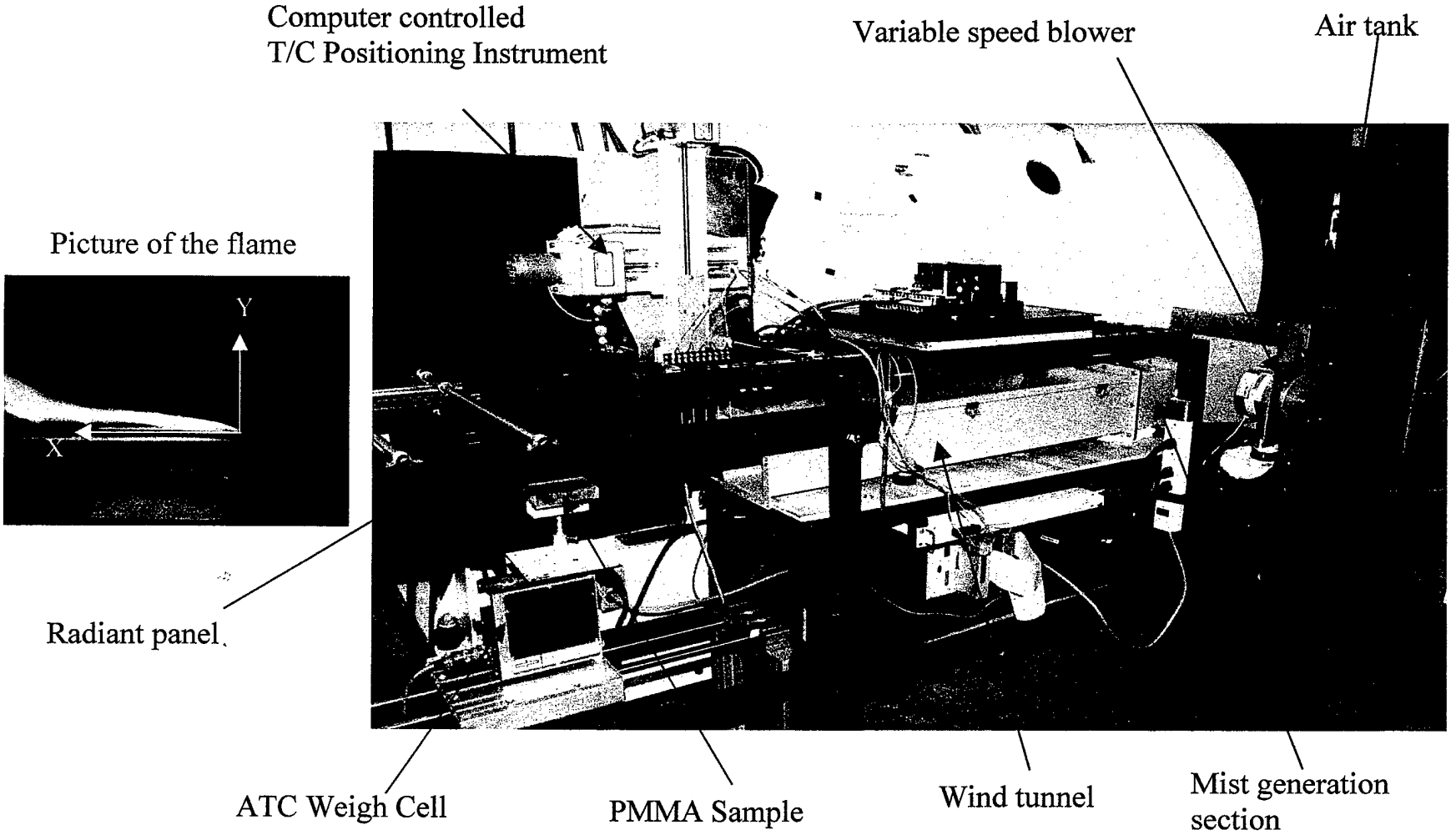

Figure 2: Picture of the Experimental setup . Insert is a picture of a typical flame

2.1.1 Temperature measurement

As the PMMA sample burns, its surface regresses with time and the flame moves down accordingly. Although surface regression is not uniform along the sample length, the surface can be estimated to regress at about 1 mm/min and if the flame moves down at that rate, it is necessary to complete the temperature mapping across the flame in under 1 min to avoid significant errors in the measurement. At the same time it is necessary to allow enough time (≥ the thermocouple time constant) during each measurement for the thermocouple bead to attain thermal equilibrium with the surrounding gases. For a 50 μm diameter thermocouple the bead diameter (butt-welded) is about 125 μm and the time constant is approximately 30 ms. [12]. Since the temperature gradient is very large within the boundary layer, measurements need to be made at very short distance intervals. Twenty measurements at 0.5 mm intervals were made across the flame at each X location to map the temperature within the boundary layer, whose width is ~ 10 mm in the trailing section. To accomplish all these requirements in less than 1 minute, the data acquisition system was programmed to acquire data at the rate of 20 per second and 20 samples were averaged per recorded data. With the travel time of the thermocouple and the processing time, the temperature mapping across the entire flame was completed within 45 seconds.

Since the thermocouples were crossing regions of high temperature gradients, the measurements are expected to include conduction errors. To minimize this error we chose very fine thermocouples with diameter of 50 μm. The conduction error with these thermocouples is expected to be small since the heat transfer area (the cross sectional area of the thermocouple) is very small. No corrections were made in the data for conduction error. However, the temperature values are corrected for thermocouple bead radiation and the details about the correction are given in our previous report [13]. For the 50-μm-diameter thermocouple a typical radiation correction at 1800 K is +62 K.

3.0 RESULTS AND DISCUSSIONS

As the airflow exits the tunnel, it expands and its velocity is expected to decrease slowly with distance from the tunnel exit. Since the sample sits close to the exit of the tunnel, it is important to ensure that the flow velocity has not dropped significantly within the length of the sample. A typical velocity profile measured with a hot wire anemometer at three locations over the sample, namely, at the beginning of the leading plate (tunnel exit), at the leading edge of the sample and at the trailing edge of the sample (4 cm and 14 cm, respectively, down stream from the tunnel exit) are shown in Fig.3. Figure 3 shows that the air velocity has not dropped significantly within the measurement location except within the momentum boundary layer (height above the sample < 10 mm) near the trailing edge. In this zone the anemometer measured the velocity in the boundary layer, which of course is lower than the free stream velocity. For example, at the trailing edge the velocity at Y = 5 mm from the sample surface is lower than the velocity measured at the leading edge of the sample or at the exit of the tunnel. These data indicate that placing the sample outside the wind tunnel so as to gain easy access to the flame is not expected to affect our results.

3.1 Gas Phase Temperatures Measurements

Figure 4 shows a typical temperature mapping of the boundary layer diffusion flame on a black PMMA sample at five X locations, 10 mm, 21 mm, 37 mm, 58 mm and 79 mm from the sample leading edge. The free stream velocity U_∞ was 84 cm/s and the flame was anchored at the leading edge during the test. All the data have been corrected for thermocouple bead radiation. After this correction, the error in the measurement varies with location in the flame. Near the peak temperature location, the error is of the order of ±40 K. Above the peak location toward the free stream, the error is higher because of instabilities, but below the peak location toward the sample surface the error decreases below ±40K. Indeed, it is about ±10K in the molten region. Generally the error is least in the leading section and highest (about ±150K) in the plume zone near the trailing edge where buoyancy effects are significant and the flow fluctuates a lot more.

In Fig. 4 the measured peak temperature increases with X from the leading edge because of convection. A maximum peak temperature of the order of 1900 ± 40K occurred at about 21 mm from the leading edge and thereafter the value of the peak temperature decreases signaling the end of the heat release region and the beginning of the plume zone. It dropped by about 200 K close to the sample trailing edge. In a related study Holve and Sawyer [14] measured a peak temperature of 1770K (uncorrected for radiation) in a PMMA opposed flow diffusion flame using 75 μm diameter thermocouples with oxidizer flow velocity of 75 cm/s. Although their configuration is different from the current one, their results are consistent with the current results.

In Fig. 4, the heights above the sample are distances between the sample surface and thermocouple bead before the flame was ignited and the surface began to regress. Temperature mapping is initiated after ignition under the radiant panel and the burning sample was moved to the exit of the tunnel and the flame had stabilized. Thus, temperature measurements were started about 1 minute after ignition and completed within the second minute. Within this time significant regression has taken place in the leading section (as we shall show later), where the heat feedback is very high. Hence, the first thermocouple, which was 10 mm from the leading edge, could not reach the molten surface of the sample since the surface had regressed. The other thermocouples got into the molten layer where they measured temperatures in the range of 630K in the trailing section and 680K in the leading section. It seems that the molten layer temperatures are slightly higher in the sample leading section since the error in the measurements in the molten layer is small, approximately ±10 K. This is expected, since it has been shown that the pyrolysis temperature increases slightly with the heat flux to the surface [10] and heat feedback is several times higher in the leading section than in the trailing section.

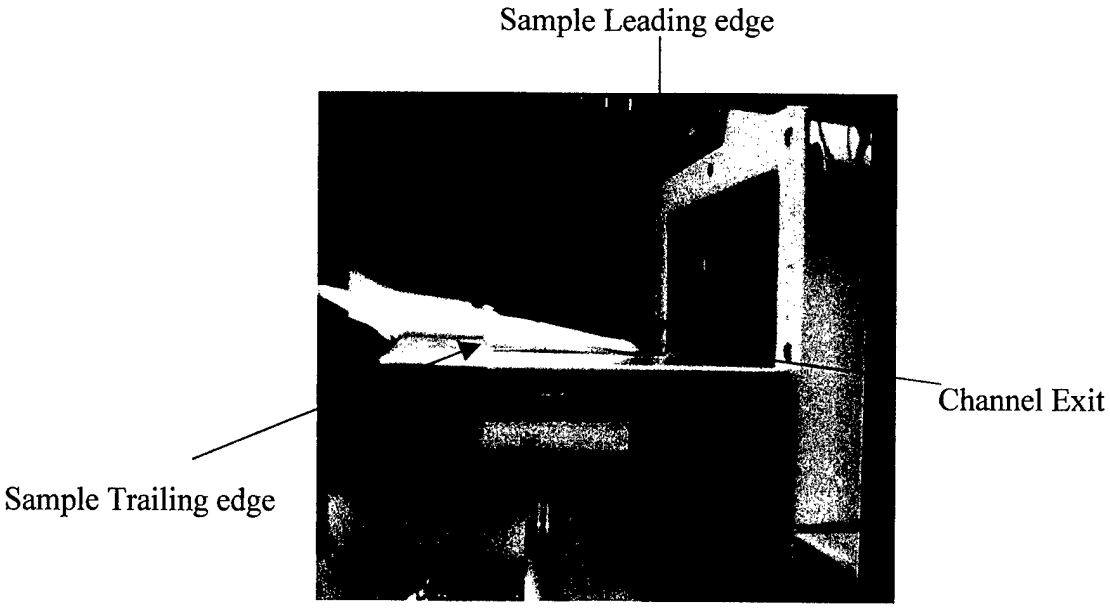

Picture of the sample holder and the flame.

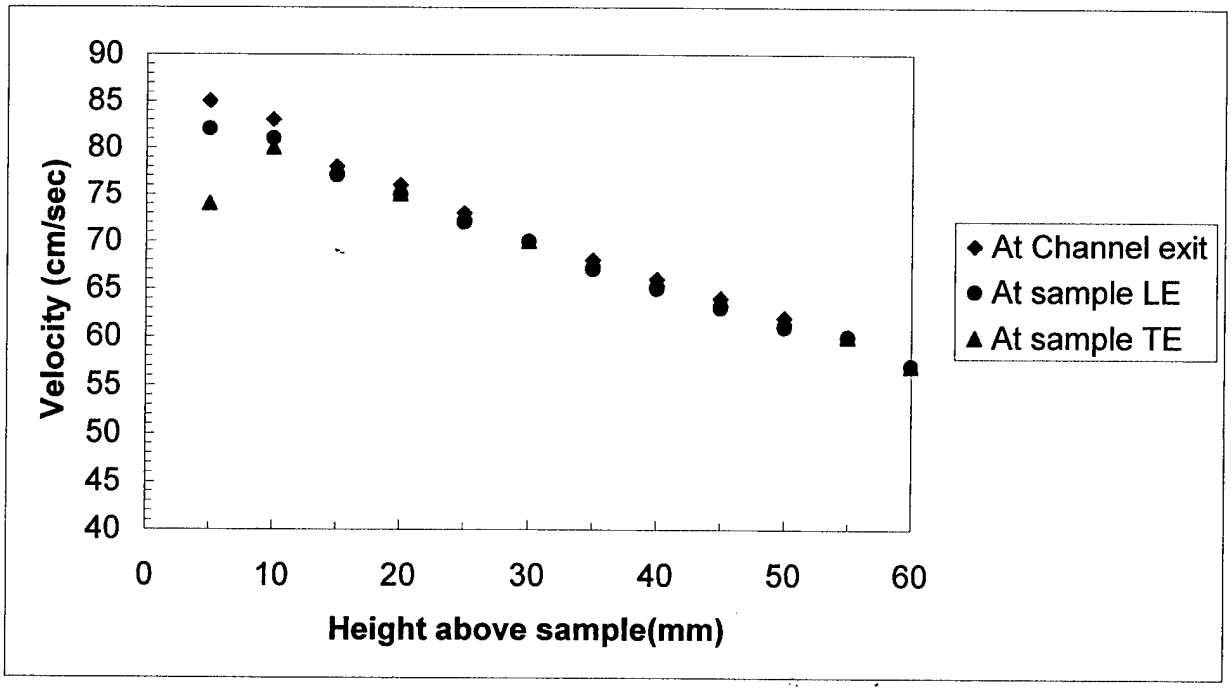

Figure 3: Air velocity at various points above the sample surface at the tunnel exit, at the sample, leading edge and at the sample trailing edge. Above: Picture of the flame and sample holder showing the measurement locations.

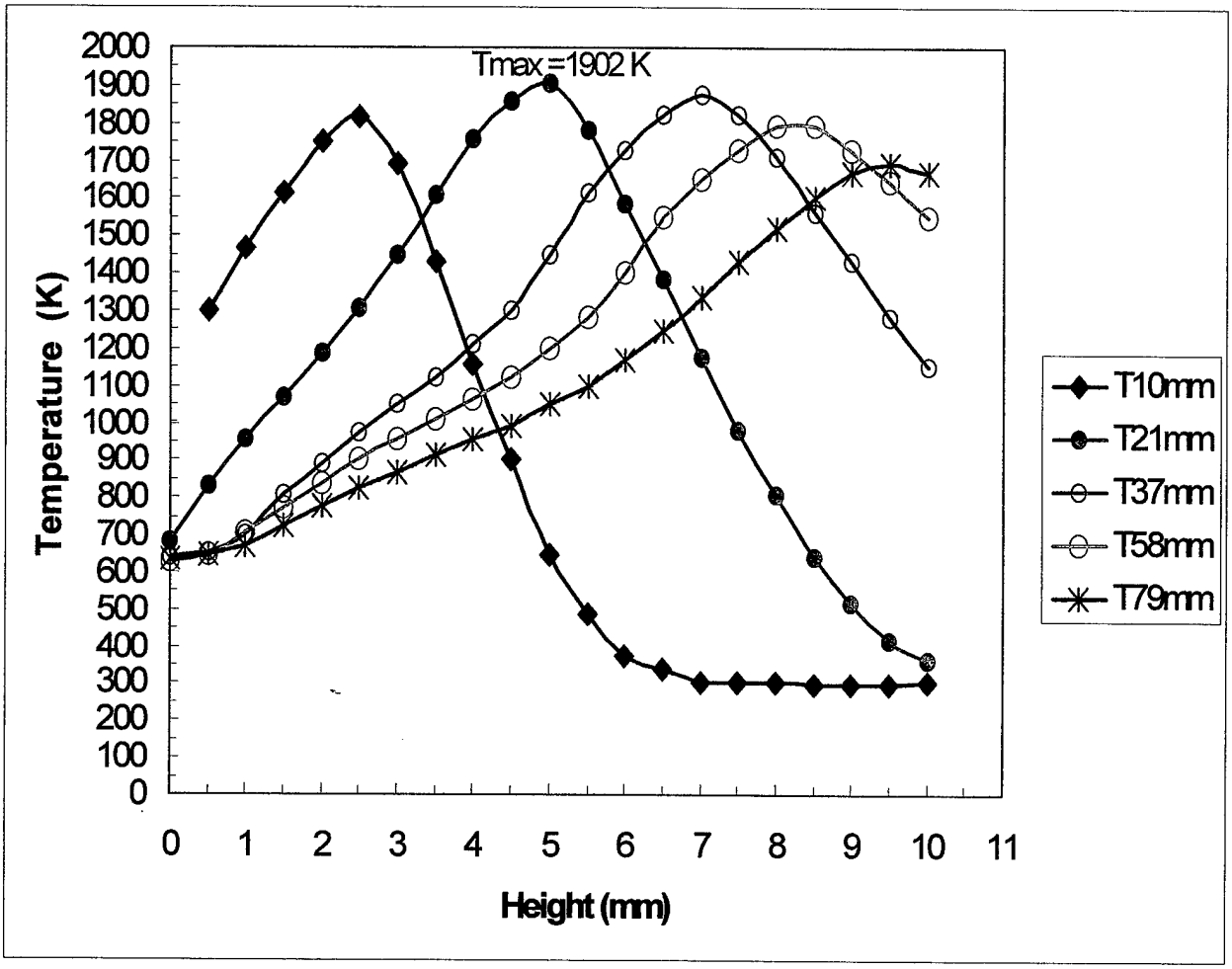

Figure 4: Gas Phase temperature profiles at various X locations along the sample with free stream velocity of 84 cm/s

A comparison of the shape of the temperature profiles at various stream-wise locations, reveals (qualitatively) that the temperature gradient decreases (flame is fatter) with distance, X from the leading edge. This is consistent with the known characteristic of boundary layer flames that heat feedback decreases sharply with X. It follows, therefore, that the surface burning rate, which is driven by the rate of heat feedback from the flame, will decrease sharply with X as will be presented later.

The heat feedback to the surface, $h\Delta T = \lambda dT/dy$ at y=0, can be approximated as $\lambda\Delta T/\delta$, where h is the net heat transfer coefficient, λ is the gas phase thermal conductivity, ΔT is the difference between the peak temperature and the surface temperature and δ is the distance between the flame and the surface (flame standoff distance). This can be expressed in terms of the dimensionless Nusselt number Nu_x, where $Nu_x = hX/\lambda = X/\delta$. In a boundary layer flame the flame standoff distance increases with X and decreases with U_∞ and these variations can be expressed in terms of Reynolds number, $Re_x = U_\infty X/\nu_\infty$, where ν_∞ is the kinematic viscosity at 300K. Boundary layer theory [3] predicts that $Nu_x \propto Re_x^{0.5}$. Using the properties of PMMA measured by Orloff et al. [15] and the correlation of Glassman [16] in Emmons boundary layer formula, one can obtain that $Nu_x = 0.1Re_x^{0.5}$. To obtain the coefficient as 0.1, ΔT = 1200K, density of PMMA ρ_s = 1.19 gm/cm^3 and λ = 0.052 W/mK is evaluated at 700K [17] (surface temperature). Thus, according to Emmons's boundary layer theory, the normalized standoff distance can be expressed approximately as $\delta/X = 10/Re_x^{0.5}$. Figure 5 show the normalized standoff distance δ/X against $Re_x^{0.5}$. The symbols are the data while the line is Emmons's steady state predictions. The data are consistent with Emmons predictions, notwithstanding the above approximation and the fact that the errors in the measurement of the standoff distances were of the order of 12%. The results in Fig. 5 suggest that the gas phase has approximately attained steady state within 1 minute after ignition when the temperature measurements were made. Also, within this time the surface is still approximately flat.

The effects of inlet velocity on the gas phase temperature profiles are depicted in Figs. 6 and 7, which show the gas phase temperature profiles for tests with U_∞ = 60, 84, 120 and 168 cm/s. As velocity increases, the flow time in the leading section decreases and approaches the chemical reaction time. Eventually, the flame anchors downstream of the leading edge, pushing the heat release zone further downstream and creating a quenching distance in the leading section. This happened with the 120 and 168 cm/s tests, where the quenching distances were ~2 and ~5 mm, respectively. At these higher velocities the flame is brought closer to the surface; i.e., δ is smaller. For example with 84 cm/s at X= 35 mm, $\delta \sim 7$ mm, but with 168 cm/s at X= 35 mm, $\delta \sim 4$ mm. Thus, at each X location the burning rate is expected to increase with velocity as we will show later. Because of this increased surface regression in the leading section in the 120 and 168 cm/s tests, the thermocouples at X= 10, 20 and 35 mm did not get to the pyrolyzing surface (height = 0) during the measurement.

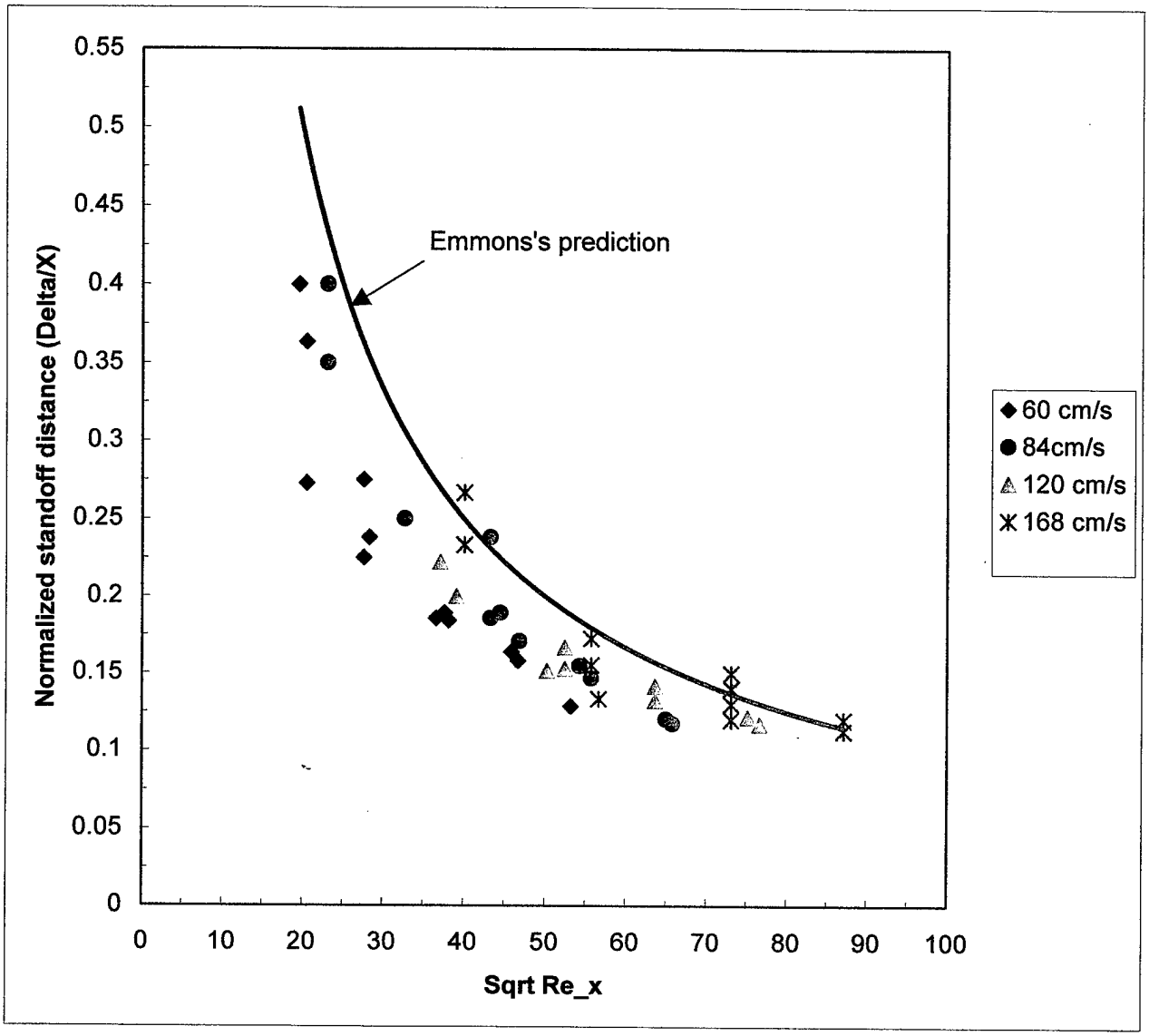

Figure 5: Normalized flame standoff distance versus $Re_x^{0.5}$

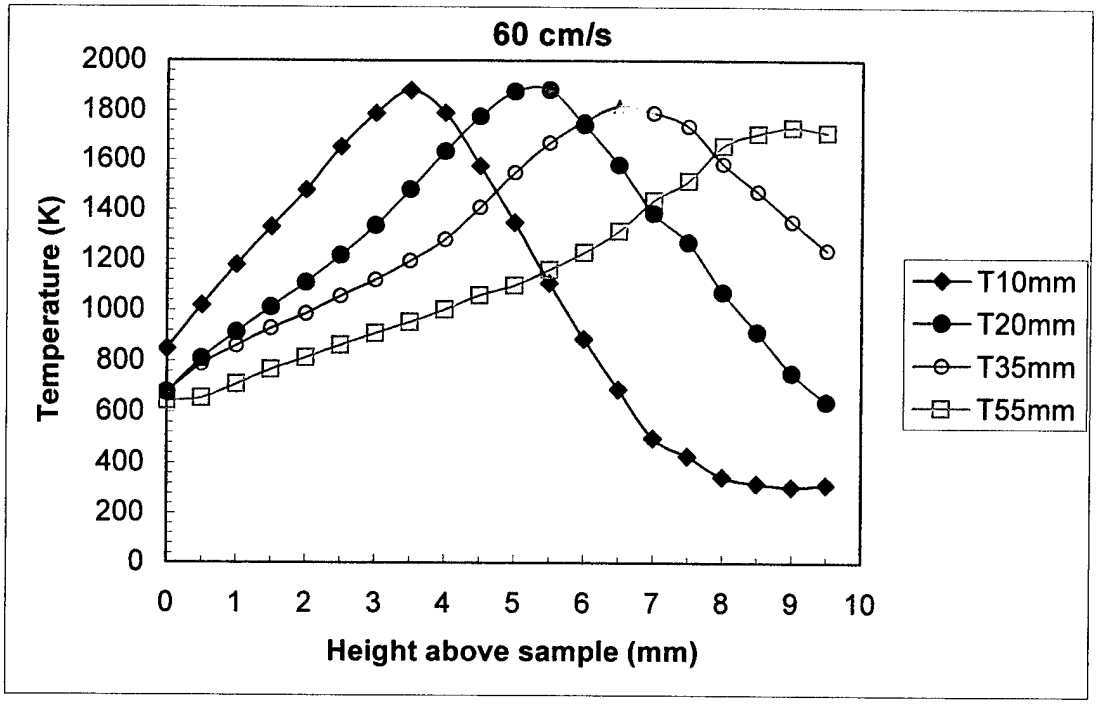

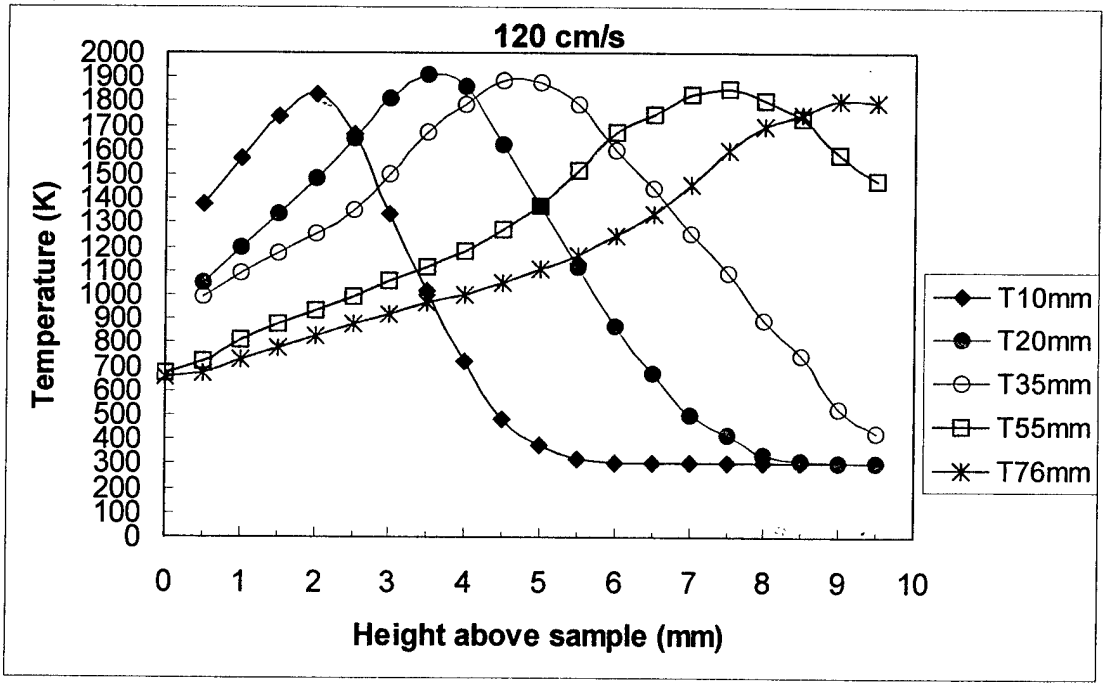

Figure 6: Gas Phase temperature profiles at various stream-wise locations with inlet velocities of 60 cm/s and 120 cm/s

close to the burning surface would be much smaller than the estimate ($\Delta T/\delta$) used in calculating heat feedback. Because of the above reasons, the calculated regression rate should be higher than the actual values. This error would be worse in the trailing section, where soot volume fraction is highest as Fig. 8 shows.

Figure 9 shows the time-averaged regression rates as a function of X for tests lasting for very short times (2.5 minutes) and U varying between 60 and 168 cm/s. Several tests with 60 and 84 cm/s were repeated to show the scatter in the data and the results at these two velocities are within the experimental error of each other. Figure 9 shows that the regression rate decreases sharply with X in the 60 and 84 cm/s velocity tests, where the flame was not dislodged from the leading edge. Indeed, the regression rate in these tests dropped by a factor of 10 as we approach the trailing edge. In both tests the peak regression rate was about 1.4 mm/min and occurred at the leading edge where the flame was anchored.

As the velocities were doubled (120 and 168) the flame was dislodged from the leading edge when it is brought to the measurement location. Recall that the flame is ignited under the radiant panel about 40 cm downstream from the measurement location. In the 120 and 168 cm/s tests, the flame re-anchored downstream from the leading edge (~2 and 5 mm, respectively) where conditions are such that the local Damkohler number Da is not below the critical value. From there the flame spread slowly upstream, decreasing the quenching distance during the test. We have shown in another paper that this is possible because of the moving boundary effects, which resulted in the creation of a stabilizing step [22]. In the 168 cm/s test, the flame hardly spread to the leading edge within the 2.5-minute test period. In the 120 and 168 cm/s tests, the cumulative effects of peak heat feedback could not be achieved at one location, since the flame "attachment" position was moving upstream with time. Therefore, the measured peak regression rates were less than the 1.4 mm/min measured at low velocities.

Figure 9 shows that the measured regression rates more than doubled as the inlet velocity was doubled (120 and 168 cm/s tests), except very near the leading edge (X < 3mm). It is interesting to note that the change in regression rate between 60 cm/s test and the 84 cm/s test is insignificant. Similarly, between 120 cm/s test and 168 cm/s test the change is also insignificant. However, the change is huge between 84 and 120 cm/s. This is because the hot gases are brought closer to the surface (δ decreased) when the inlet velocity increased. This was shown in Fig. 5 where the normalized standoff distance decreased with Re_x. The decrease in the thermal boundary layer thickness leads to increased convection transport and consequently a higher regression rate. Tables of regression rate data at various velocities and test durations are presented in the appendix.

The mass flux at any X location can be obtained from the regression rate and PMMA solid density. Figure 10 shows the percent of mass burned up to a stream-wise location versus the normalized distance from the leading edge for a 5-minute test. This percentage is the ratio of the sum of the sample mass lost up to that location divided by the total mass lost in the entire length of the sample during the test. The results show that most burning takes place in the leading section as a result of the non-uniform heat feed back inherent in boundary layer diffusion flames. For example, during the five minutes, about 85% of the mass loss occurred in the first 50% of sample length and nearly 40% of the mass loss took place in the leading 10% of the sample

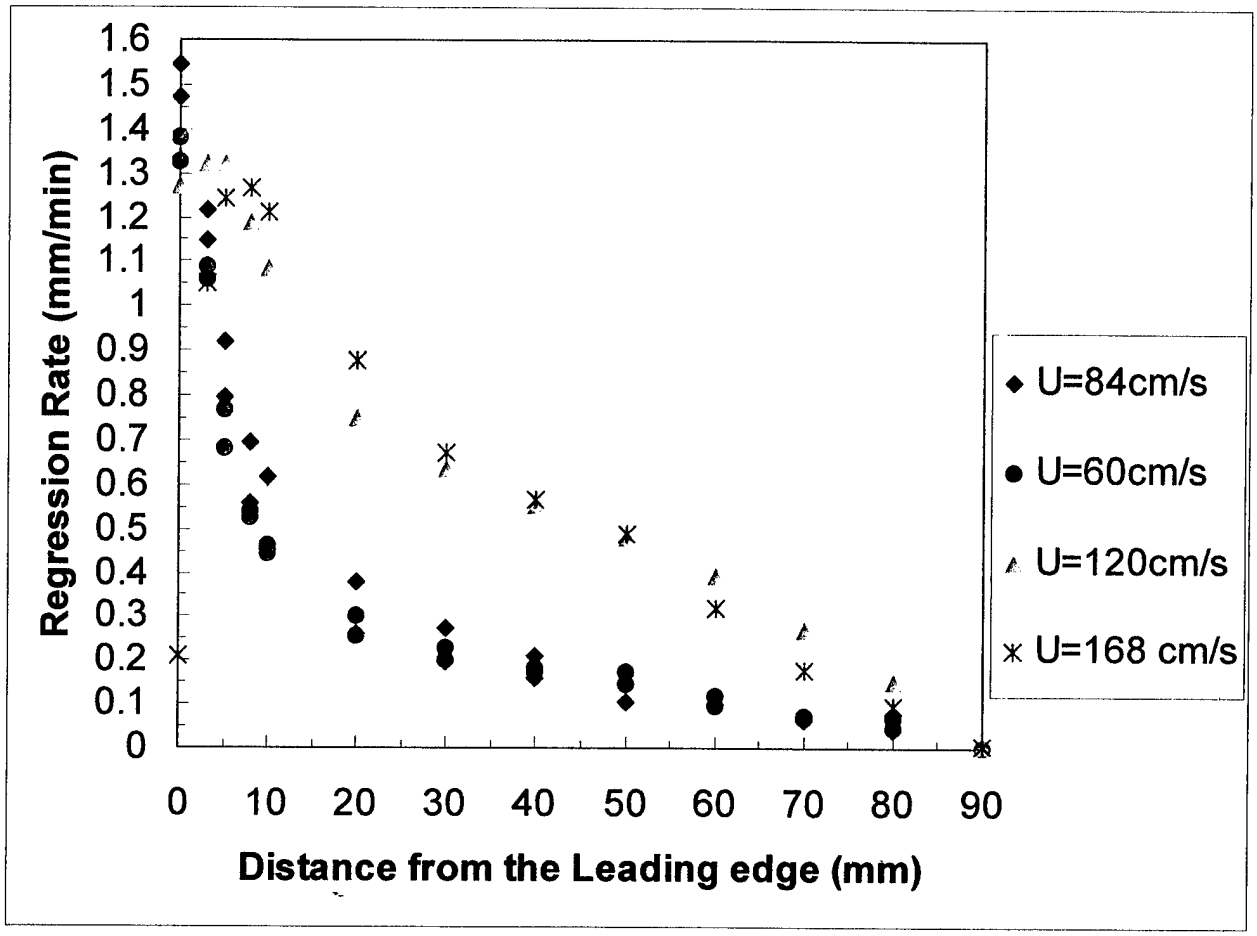

Figure 9: Surface regression rate with X in 2.5 minute tests at various Free stream velocities

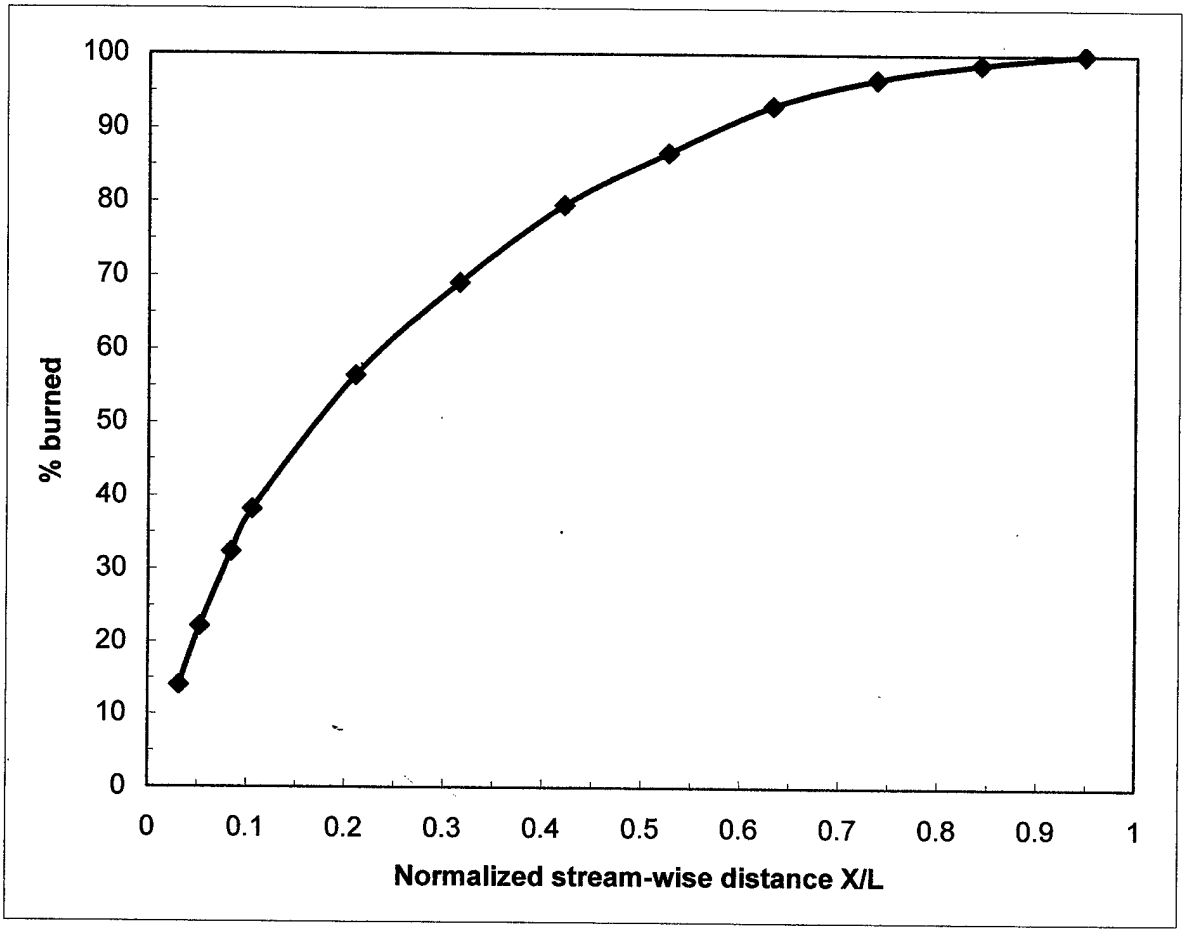

Figure 10: Fraction of the burned mass contributed by the various sections of the sample, Test duration = 5 min, U = 84 cm/s

length. This shows that the burning rate is disproportionately higher in the leading section than downstream. To obtain optimum suppression in a boundary layer flame this result suggests that it is necessary to deliver the suppressant in the leading section where its effect will be more significant.

3.3 The Effects of non-uniform Moving Boundary on the local Burning Rate

Figure 11 shows the cross-section of the PMMA samples at the end of experiments that lasted 5, 10 and 20 minutes. In each case the surface had regressed unevenly along X from its original flat profile. Furthermore, much higher regression took place in the leading section compared to downstream. This reflects the non-uniform rate of heat feedback to the surface. Within 5 minutes into the experiments the sample receded below the level of the leading plate (see Fig.2 insert). This results in the formation of a valley or a step in the leading section as shown in the pictures in Fig. 11. Figure 11 shows that as time progresses the valley gets deeper and the position of the deepest point moves slightly downstream. This suggests that the location of the smallest flame standoff distance is moving slowly downstream. Indeed, in 5 minutes the surface is still flat near the trailing edge and becomes increasingly curved as time progressed. Non-uniform surface regression lead to the formation of a valley that gets deeper with time. This has two significant effects. First the local burning rate in the leading section where the valley is deepest decreases with time. Secondly, the presence of the valley enhances flame stability and its ability to spread upstream. This effect was discussed in detail in our previous report [22]

The time-averaged regression rate with stream-wise location X at various times is presented in Fig. 12. These tests were conducted with normal air at free stream velocity U_∞ of 84±1 cm/s and test durations of 5, 7.5, 10, 15, and 20 minute. Several tests were repeated to show the scatter in the data. Figure 12 shows that the regression rate peaks near the leading edge and thereafter decreases sharply with X. The rate also decreases sharply from the peak toward X = 0, especially at large times due mainly to heat losses to the holding container at the sample leading edge.

Figure 12 shows that the regression rate decreases with time in the leading 10 mm of the sample. For example in a 5, 10, 15 and 20-minute tests, the regression rates at X = 5 mm are 0.90, 0.70, 0.55 and 0.45 mm/min, respectively. Furthermore, the peak regression rate decreased by a factor of two between the 5 and 20-minute tests. Indeed, Fig. 12 shows that the surface regression decelerates with time in this section as the surface profile in this section deepens and widens (Fig. 11). In Fig. 12 the X position of the peak regression rate shifted slightly downstream with time corresponding to the slight shift in the position of the deepest point in the valleys in Fig. 11. Therefore, one can infer from Figs 11 and 12 that the uneven surface regression and creation of a valley is related to the transient surface regression rate in the leading section. Far from the leading edge (X > 30 mm) where the heat feedback had decreased substantially, the degree of surface regression is small; hence, the effects of uneven moving boundary are expected to be very small. Further downstream in the trailing section, there is no discernable trend with test duration in the data, although the regression rate for the 20-minute test is the largest at each X location. This may suggest a slight increase in regression rate in this section. This will be discussed in more details later but first we present a discussion of the transient burning rate in the leading section.

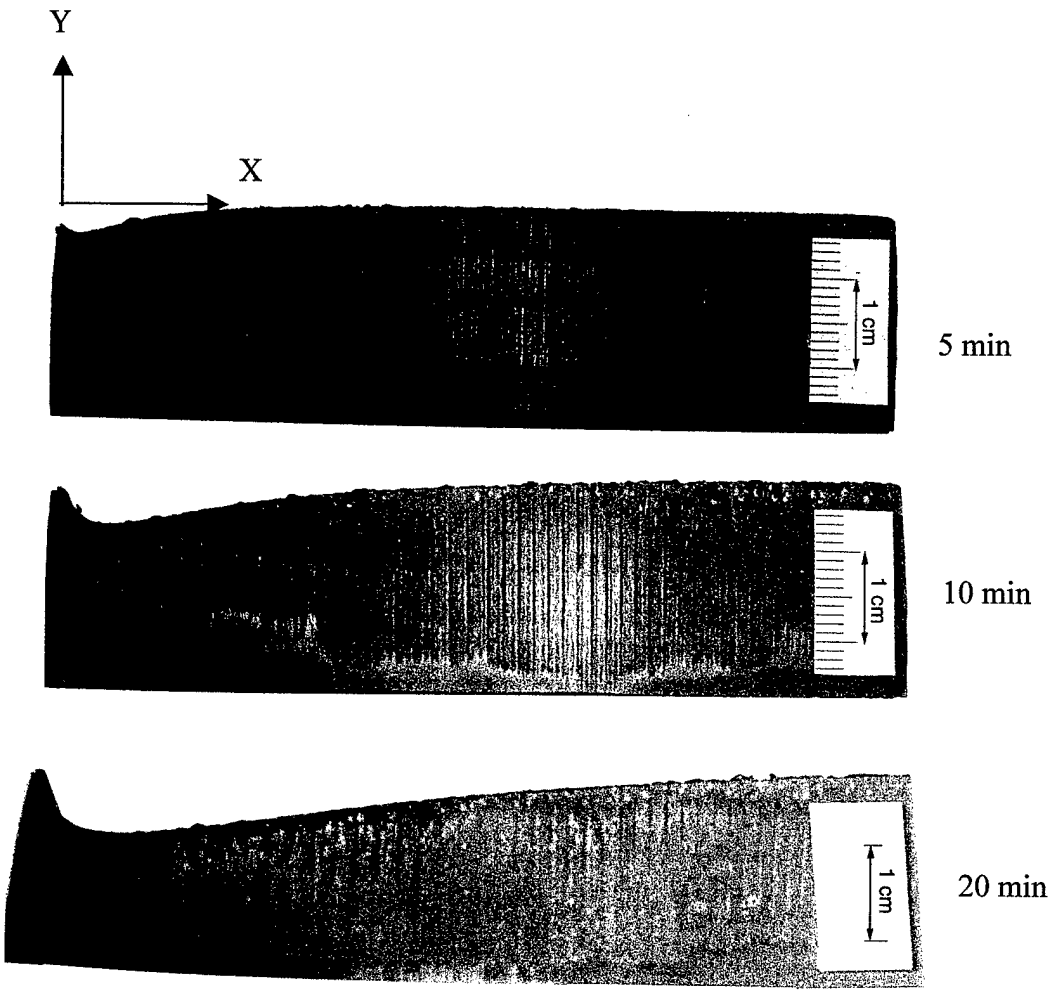

Figure 11: PMMA sample surface profiles after 5, 10 and 20-minute burn

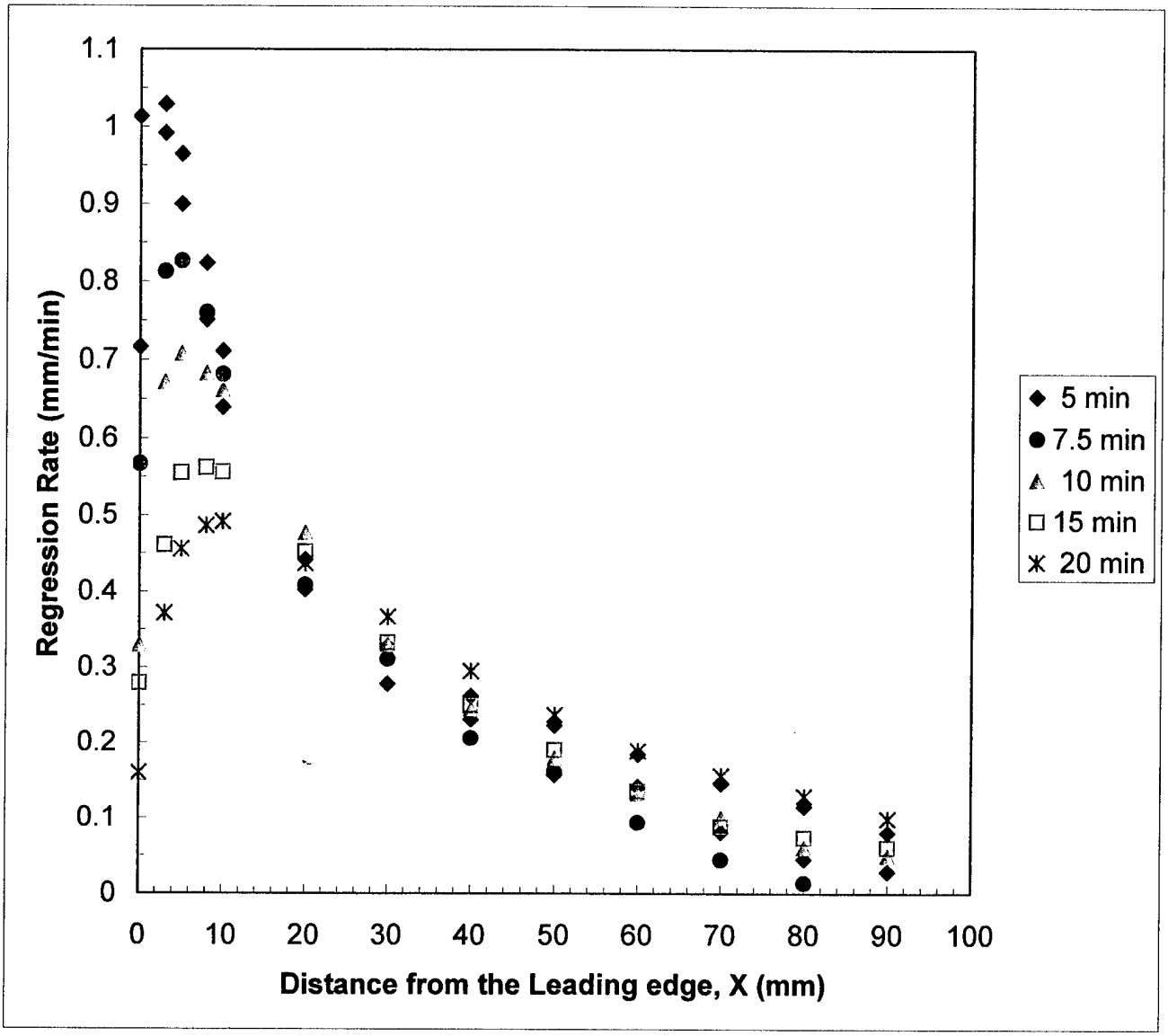

Figure 12: Variation of PMMA surface regression rate with time at various locations along the sample length. U=84 cm/sec.

3.3.1 Transient Burning rate in the Leading section

The deceleration of surface regression in the leading section shown in Fig. 12 implies that the heat feedback to the surface in this section decreases with time. Experiments were performed to determine the heat feedback to the sample surface in the leading section at various times. With one R-type thermocouple, 125 μm diameter located at X=5 mm from the sample leading edge, temperature profiles across the flame were measured at 1, 5,10, 15 and 20 minutes into the test. At these times, the thermocouple was moved across the flame making temperature measurements at 0.5 mm intervals until it entered the PMMA melt layer whose temperature was about 650K. Figure 13 shows the temperature profiles measured at different times. It shows a peak temperature of the order of 1400K, which is quite low compared to what one would measure with a finer thermocouple. A 125 μm diameter thermocouple was chosen to ensure that the thermocouple would penetrate the melt layer without bending. The flame standoff location (δ) can be estimated in each profile as the height of the peak temperature above the surface. Figure 13 shows that the flame standoff location increases with time. For example, the flame standoff distance increased from 4 mm in the first 5 minutes to about 5.5 mm in about 20 minutes. Also, within the same time the peak temperature dropped from about 1400K to about 1200K. The profiles also show (qualitatively) that the temperature gradient close to the surface decreases with time. These data strongly suggest that the heat feedback to the sample surface is decreasing with time as the valley deepens.. Generally, it is assumed that the flame moves down with the regressing PMMA surface. However, the current results indicate that as time progresses the flame does not keep up with the surface as it regresses in the leading section. Thus, the heat feedback to the surface decreases with time in the leading section, giving rise to the regression rate decreasing with time. Although the temperatures measured with the 125 μm-diameter thermocouple are quite low compared to what we had measured with finer thermocouples in Fig. 4, it is expected that this did not affect the trend observed in the data and therefore the conclusions reached with these data would not change.

Furthermore, it was observed that the flame near the leading edge was bluish right after ignition when the leading section of the sample is still flat. This is an indication that a more efficient mixing of oxygen and fuel was obtained in this region of the flame at this stage. However, as the test progressed and the valley formed and deepened, the length of this blue portion shrank, suggesting that the moving boundary effects resulted in a leaner fuel/oxygen mixture in this section with time. One could speculate that because of the valley, the combustion products in the valley are not swept away as readily as was the case when the surface was flat. Hence the oxygen mass fraction within the valley would decrease as the valley deepens. This would result in a drop in flame temperature (as shown in Fig. 13) and consequently a drop in heat feedback to the surface.

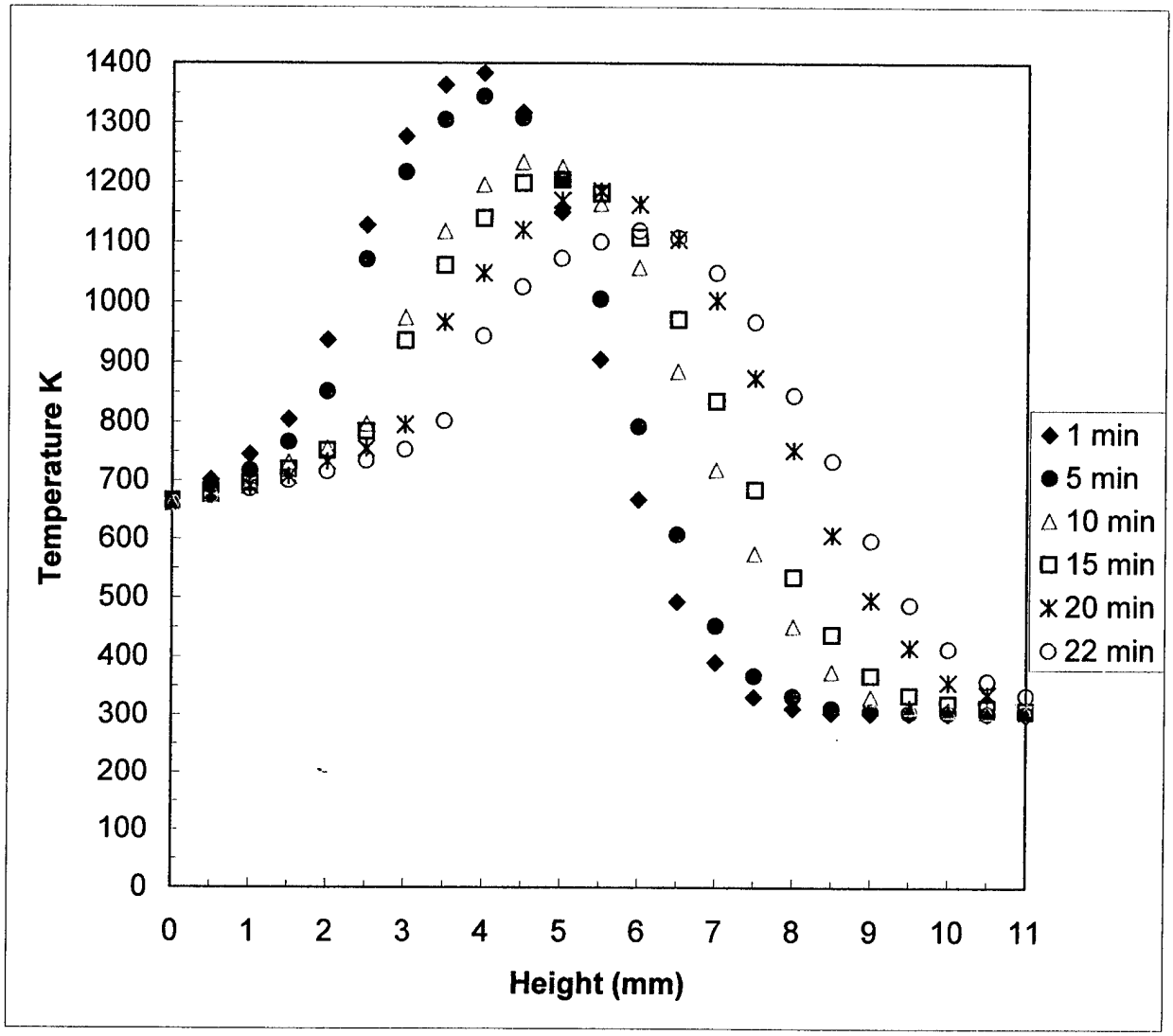

Figure 13: Temperature Profiles at various times at X = 5 mm as the valley deepens in this location.

As the sample burns, heat is lost to the sample holder through the sides and from the bottom surface after the thermal boundary layer in the solid reaches the back surface. A set of tests was conducted to investigate the role of the heat losses on the unsteady regression rate near the leading edge. The quartz plates were replaced with heat resistant felt material. The thermal conductivities of quartz glass and felt are of the order of 1.7 W/m K and 0.07 W/m K, respectively [23], thus using felt instead of quartz glass reduces the heat losses by a factor of about 24. Figure 14 summarizes the results of tests with insulation. In the 5-minute test the peak regression rate occurred at the sample leading edge, where the flame was anchored within this time. Because of the insulation the flame tends to attach very close to the leading edge even at longer times. Thus, in 10 and 20-minute tests the regression rate did not decrease as sharply toward the leading edge as was the case with quartz glass (Fig. 12) as a result of reduced heat losses. Figure 14 shows that the regression rate near the leading edge was time dependent even when heat losses to the edge and back were significantly reduced. Recall that the sample holder has a leading plate and as the sample surface regresses below the leading plate level a valley is formed, which deepens with time. Hence, the regression rate in the leading section (especially, $10 < X$) decreases with time like in Fig. 12. The measured peak regression rates with the insulated leading edge were similar to those measured with higher heat losses (Fig. 12). However, when both leading edge and sample bottom were insulated, the peak regression rate increased significantly in the 20-minute test. This is an indication that the thermal boundary layer in the solid has reached the back surface in the leading 10 mm within the 20 minutes. The results presented in Fig. 14 indicate that the decrease in regression rate with time in the leading section was caused by the presence of the valley and that heat losses at the leading edge or at the bottom had no significant effects on the transient behavior.

3.3.2 Transient burning rate in the trailing section

As noted earlier, it seems from Fig. 12 that the regression rate slightly increases with time in the trailing section. This transient burning downstream is suspected to be due to solid phase transient heating. During ignition the entire surface is heated up at a very high rate and then ignited to obtain a stable boundary layer flame within 1 minute. Then, the external heat is turned off and the heat reaching the surface in the trailing section drops very significantly (by about 10 times). Meanwhile in the leading section where the surface is closest to the flame the heat feedback is high enough for pyrolysis to continue at a high rate. However, in the trailing section where the heat feedback is now much lower (more than 5 times lower), solid phase transient effects are significant. Hence, it takes significant time (order of minutes) for the solid to heat up again and start pyrolyzing at a significant rate. Vovelle et al. [10] measured solid phase temperatures and total mass loss rate in non-flaming pyrolysis experiments with vertical PMMA samples. They showed that the time for the surface to reach pyrolysis temperature and steady state total burning rate decreased with the exposed radiant heat flux. Similar results were reported by Tewarson and Pion [11] for the pyrolysis of PMMA in a horizontal configuration.

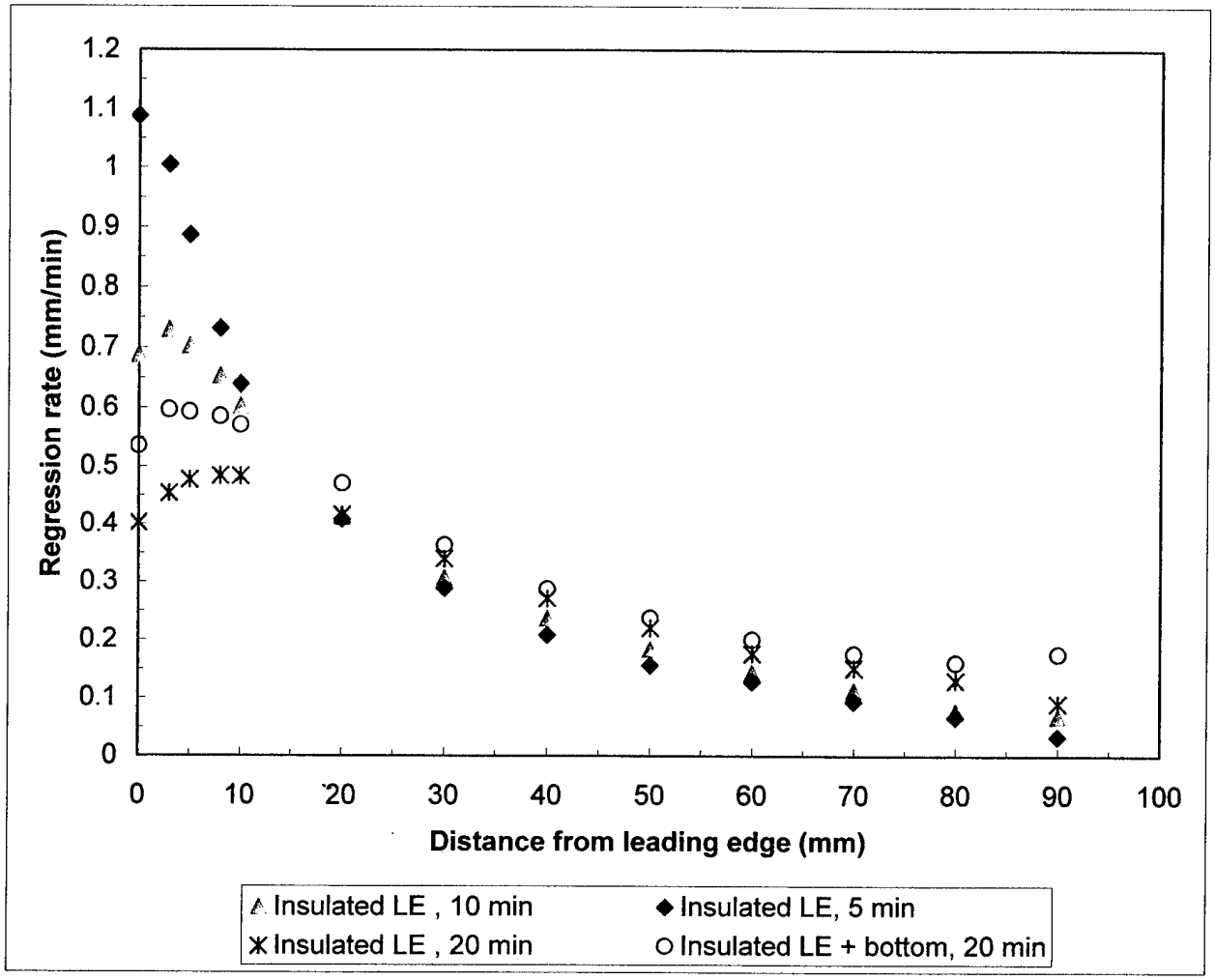

Figure 14: Effects of heat transfer in the Leading edge on the Regression Rate, U_∞ = 84 cm/s

Furthermore, at the beginning of a test, after the radiant panel is turned off, the bubbling intensity can be seen to decrease along the length of the sample, with smaller and tightly packed bubbles in the leading section and bigger and fewer bubbles far from the leading edge. A front can be seen, behind which there was intense bubbling and ahead of which there was very little gasification. Thus, at the beginning of the test there is a zone of very little gasification near the trailing edge and the size of this zone diminishes with time as this part of the sample gets heated up. Figure 15 shows pictures of PMMA surfaces, which burned for 2.5 and 5 minutes in tests with U=168 cm/s. It clearly shows that within 2.5 minutes the edge of the front had not extended to the trailing edge. However, within 5 minutes, the front had reached the trailing edge. As this front spreads in the co-current direction, the regression rate in the trailing section increases. This was responsible for the observed increase in burning rate in the trailing section. Because the heat feedback in the trailing section is small, the heat-up rate is slow and the measured increase in regression rate is very small at the current test conditions. At these conditions, this increase seems to be within the experimental error (Fig. 12). However, the increase can be seen more clearly in terms of integrated burning rate shown in Table 1.

Table 1 shows the variation of the integrated burning rate (BR) over the entire sample, in the leading section ($0<X\leq 20$ mm), and in the rest of the sample ($20<X\leq 90$mm), with time. Here burning rate is obtained as $\sum \rho R \Delta X Z$, where, ρ is the PMMA solid density (1.19 gm/cm^3); R is the local regression rate; Z is the sample width (7.5 cm); ΔX is a small increment in X associated with R and the summation is between the limits in X. Table 1 shows that the integrated burning rate decreases with time in the leading section (as expected), while it increases with time in the trailing section. Thus, in Fig. 12, the local regression rate downstream actually increased with time but this could not be shown clearly in Fig. 12 because the increase is very small. However, when the small regression rate is summed over a large area ($20<X\leq 90$ mm), the increase in burning rate becomes quite significant (about 50% between 5 and 20 minutes). Table 1 also shows that the burning rate integrated over the entire plate does not vary much with time. It varied only between about 1.88 and 2.1 gm/min in this case. Thus, the decrease in burning rate in the leading section seems to be compensated approximately by the increase in the burning rate in the trailing section in this case. Whether this is real or a coincidence needs to be investigated further.

In addition, it is suspected that the downward movement of the flame as the surface regresses could contribute to the slight increase in regression rate measured in the trailing section. This would imply that the flame would move closer to the surface with time and therefore the heat feedback to the surface would increase with time. To test this, temperature profiles across the flame in the trailing section, 80 mm from the leading edge, were measured at various times during the test. We used R-type thermocouple, 75 μm diameter for this set of tests and the results are shown in Fig. 16. Figure 16 shows that the peak temperatures remain unchanged with time but the flame standoff distance decreased from about 8.5 mm in 1 minute to about 5.5 mm in 20 minutes. Thus, it seems that in the trailing section, the flame moved closer to the surface with time and this would lead to an increase in heat feedback to the solid with time, contributing to the observed increase in burning rate.

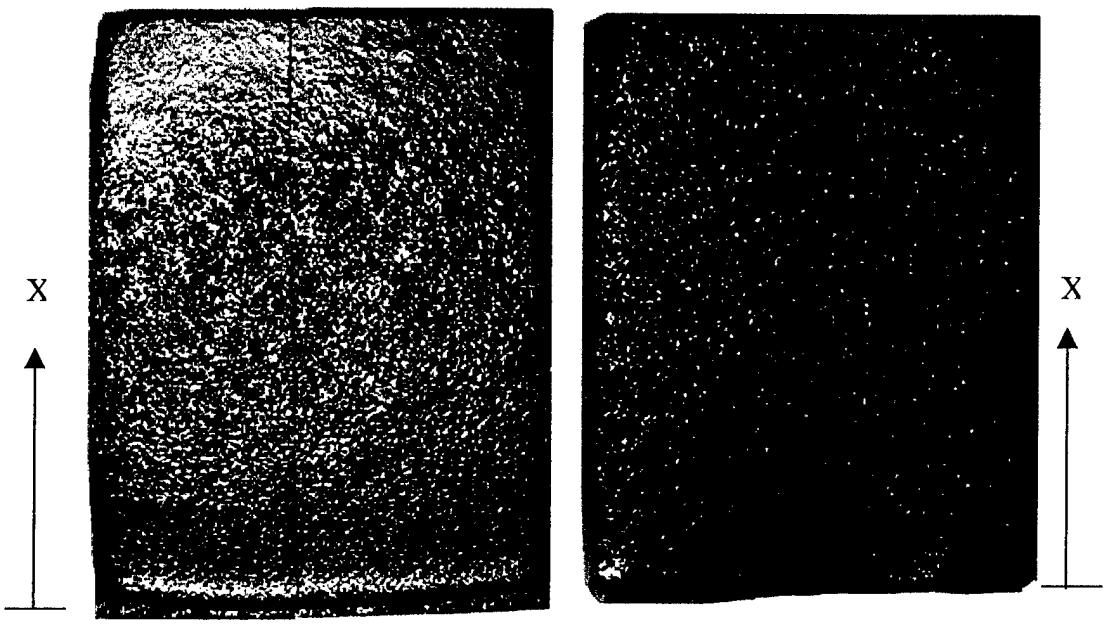

Figure 15: Pictures of PMMA surfaces after 2.5 and 5 minutes burn. U_∞ = 168 cm/s

Table 1: Stream-wise integrated Regression rate (BR), Total BR ($0 \leq X \leq 90$); in the Leading section ($0 < X > \leq 20$ mm) and Downstream ($X > 20$ mm) $U_\infty = 84$ cm/s,

Test Time (min)	Total BR, ($\sum R \Delta X \rho Z$), entire surface (gm/min)	BR, $0 < X > \leq 20$ mm (gm/min)	BR, $X > 20$ mm (gm/min)	% of total BR $0 < X \leq 20$ mm	% of total BR beyond 20 mm
5	1.97	1.11	0.86	56.3	43.3
5	1.96	1.07	0.89	54.4	45.6
10	2.01	1.04	0.98	51.5	48.5
15	1.88	0.88	1.01	46.6	53.4
20	2.1	0.79	1.31	37.5	62.5

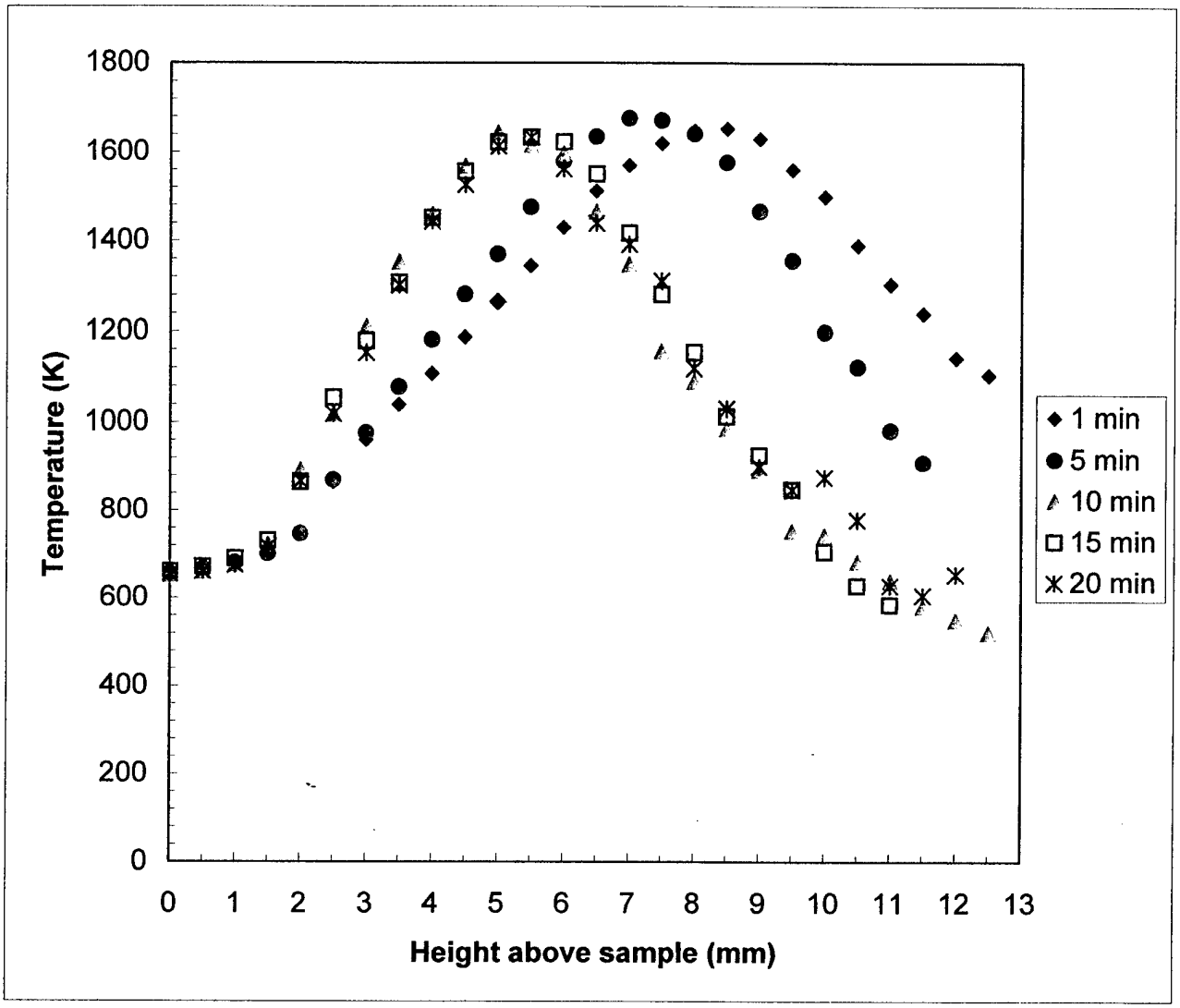

Figure 16: Temperature Profiles at various times at the center of the sample, 80 mm from the leading edge (trailing section)

At any location along the sample length, the net heat feedback from the flame ($h\Delta T$) is used to warm the solid up to the pyrolysis temperature (Q_t), as well as provide the heat of pyrolysis (Q_p). In the leading section the net heat flux from the gas phase is very large and therefore the heating up process occurs rather quickly, and $h\Delta T$ quickly approaches Q_p. However, because of non-uniform moving boundary effects, the net heat flux from the gas phase decreases with time as was shown in the previous section and therefore the heat for pyrolysis decreases with time. On the other hand, in the downstream region, where the net heat feedback is very small, the heating up process occurs slowly and hence the heat available to produce gaseous fuel increases slowly with time. In addition, the net heat feedback to the surface increases slightly with time as a result of non-uniform moving boundary effects. Thus, pyrolysis increases downstream as the sample warms up and heat feedback slightly increases. The effects of these transients on the measured local burning rate are shown in Figs. 17-20, where dimensionless burning rate Nu_x is plotted against $Re_x^{0.5}$. Here, Nu_x is obtained as

$$Nu_x = R\rho_s LX/(\lambda\Delta T); \qquad (5),$$

where $\lambda = 0.052$ W/mK (evaluated at 700K) and $\Delta T = 1200$K.

In classical boundary layer theory where moving boundary effects and solid in-depth heating are neglected, the net heat feedback equals the heat for pyrolysis and steady state solutions are obtained as $Nu_x = 0.1Re_x^{0.5}$. This solution is plotted as a straight line in Figs. 17 - 20. The classical theory also assumed infinite rate kinetics, constant properties, $Le = Pr = Sc = 1$ and zero axial diffusion. Also plotted in Figs. 17-20 are selected points in the numerical solutions of this problem by Ananth et al. [24], where all the classical assumptions were relaxed except for the moving boundary effects and the in-depth solid heat-up. Figure 17 shows the variation of Nu_x with $Re_x^{0.5}$ for free stream velocity of 60 cm/s and test time increasing from 5 to 20 minutes. The curves in Fig. 17 are approaching straight lines (steady state) as time increases. They show that steady state is attained faster in the leading section than down stream, since the heat feedback is higher in that section. Furthermore, the higher the velocity, the closer the flame stands to the surface (δ is smaller); hence the higher the heat feedback and the faster steady state is attained. For example, with $U_\infty = 60$ cm/s, steady state is approximately attained for $Re_x^{0.5} < 28$ which corresponds to $0 < X < 20$ mm and $Re_x^{0.5} < 40$ ($0 < X < 40$ mm) in 5 and 20 minutes, respectively. On the other hand with 84 cm/s free stream velocity (Fig. 18), steady state is attained within $0 < X < 30$ mm ($Re_x^{0.5} < 40$) and $0 < X < 47$ mm ($50 > Re_x^{0.5}$) in 5 and 20 minutes, respectively. However, near the leading edge ($20 > Re_x^{0.5}$) the measured burning rates are beginning to be less than Emmons's prediction at long times (>15 min). This is because the burning rate decreases with time in this section due to the effects of the non-uniform moving boundary. This shows more prominently at higher velocities (Figs. 19 and 20). Figure 18 also shows data measured by Agrawal [5] at $U_\infty = 90$ cm/s. His test duration was not reported, but it seems that he burned for longer time than we did since his data are close to steady state. His data also clearly show the effects of moving boundary in the leading section, which is another indication that the tests probably lasted longer than 20 minutes. Figures 19 and 20 show similar

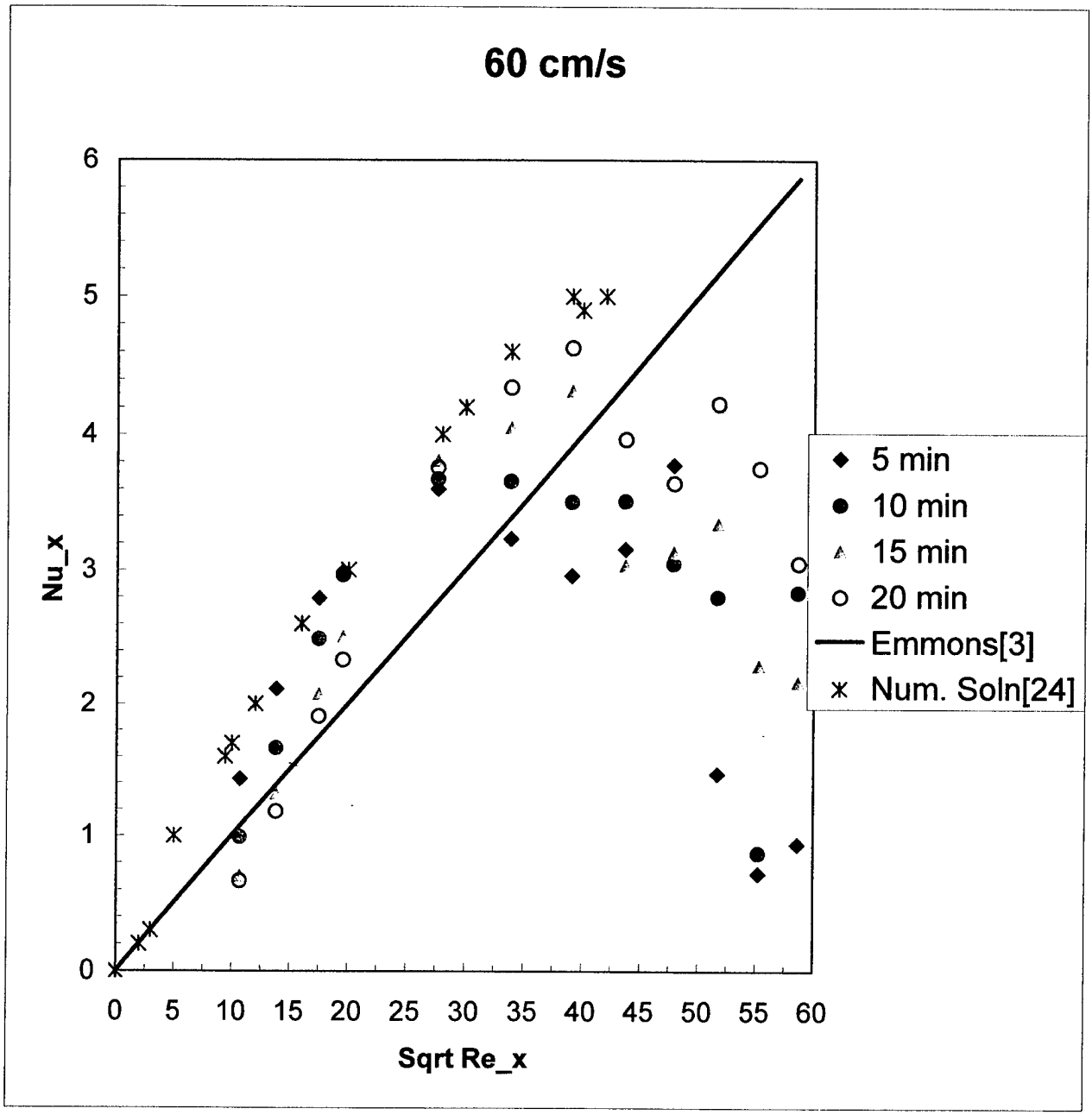

Figure 17: Normalized burning rate Nu_x versus $Re_x^{0.5}$ for U_∞ = 60 cm/s

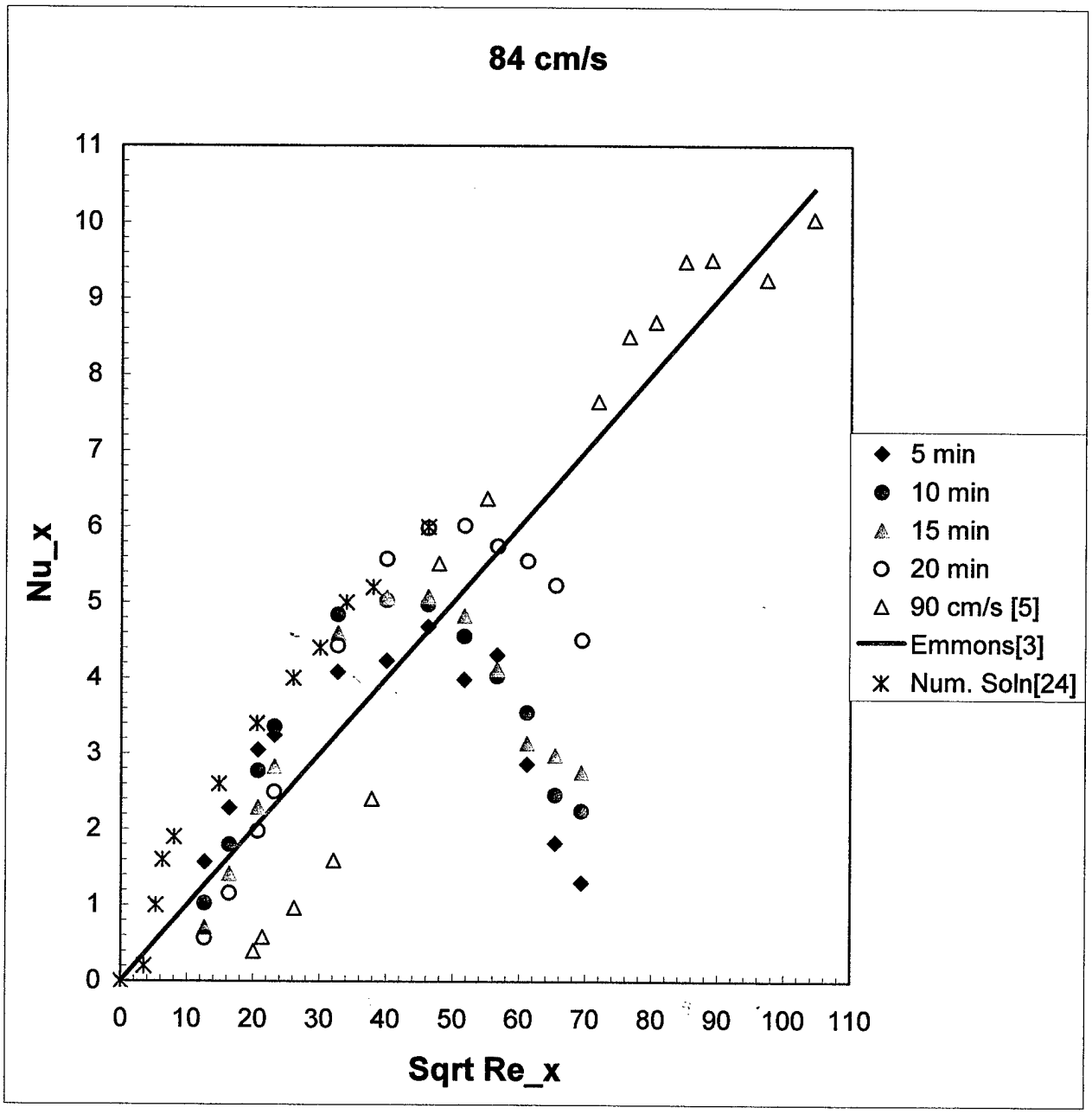

Figure 18: Normalized burning rate Nu_x versus $Re_x^{0.5}$ for $U_\infty = 84$ cm/s

plots for free stream velocity of 120 and 168 cm/s. Again one notes that the higher the velocities the further downstream the steady state front had reach at a given time. The effects of decrease in regression rate with time in the leading section are shown more prominently for $0<X<10$ mm corresponding to about $30 > Re_x^{0.5}$ in 120 cm/s test. One notes that in this region Nu_x decreased with time. For example, at $Re_x^{0.5} \sim 15$, between 5 and 20 minutes, the Nu_x decreased from 1.5 to 0.5 in the test with $U_\infty = 120$ cm/s. At 168 cm/s free stream velocity (Fig 20) the decrease in regression rate in the leading section due to the moving boundary effects occur at $35 > Re_x^{0.5}$.

However, downstream, the data show that the burning rate is nearly steady near the end of our 9.5-cm sample after about 15 minutes. On the other hand Agrawal's data at 150 cm/s show that steady state was approached within $X < 20$ cm ($140 > Re_x^{0.5}$). Thereafter, the last data point seems to suggest a downward trend. Recall that he had a 30 cm sample.

It appears that at steady state the data are close to the numerical solution and are higher than the Emmons's predicted burning rate. The under prediction could be due to the approximations inherent in Emmons's analysis, which were relaxed in the simulation. However, because the simulation did not account for moving boundary effects in the leading section, its results are increasingly higher than the data with time. Furthermore, since the numerical simulation did not include any solid phase in-depth heat transfer, the experimental data approach the numerical predictions at long times downstream (Fig. 20). At very long times and higher velocities the data could be higher than the numerical predictions because of the moving boundary effects. Recall that we have shown in Fig. 16 that the flame standoff distance δ decreases with time downstream because of the non-uniform moving boundary effects.

Also plotted in Fig. 20 in a broken line is a correlation of the data of Zhuo and Fernandez-Pello [25]. Corrections were made for the difference in the values of ΔT and other physical constants they used and the ones used in this work. They ran experiments with 37 cm X 7.6 cm X 1.27 cm PMMA samples with U_∞ varying between 100 and 400 cm/s. In their tests the flame was spreading in the co-current direction and therefore, the time the sample burned varied with X location. Nonetheless, their test duration is of the order of 20 minutes. A similar condition was obtained in Agrawal's [5] experiments. With these conditions (high U, thin sample), one would expect Zhuo and Fernandez-Pello's data to be higher than the current measurements, but their data are less than the rest of the data in Fig. 20 for $Re_x^{0.5} > 60$.

3.3.3 Transient burning rate in slow spreading flames

The transient behavior discussed above are in cases where the flame was not spreading up stream (flame attached at the sample leading edge) or there was a very short length of fuel upstream (~3 mm) at the beginning and flame spread to X=0 in less than 5 minutes. The first case refers to tests with free stream velocities of 60 and 84 cm/s, where the flame could not spread upstream beyond the leading edge because of the non-combustible material (quartz and aluminum). The second case refers to tests with free stream velocities of 120 and 168 cm/s, where a small quenching distance of about 2 mm and 5 mm, respectively, were established in the leading section.

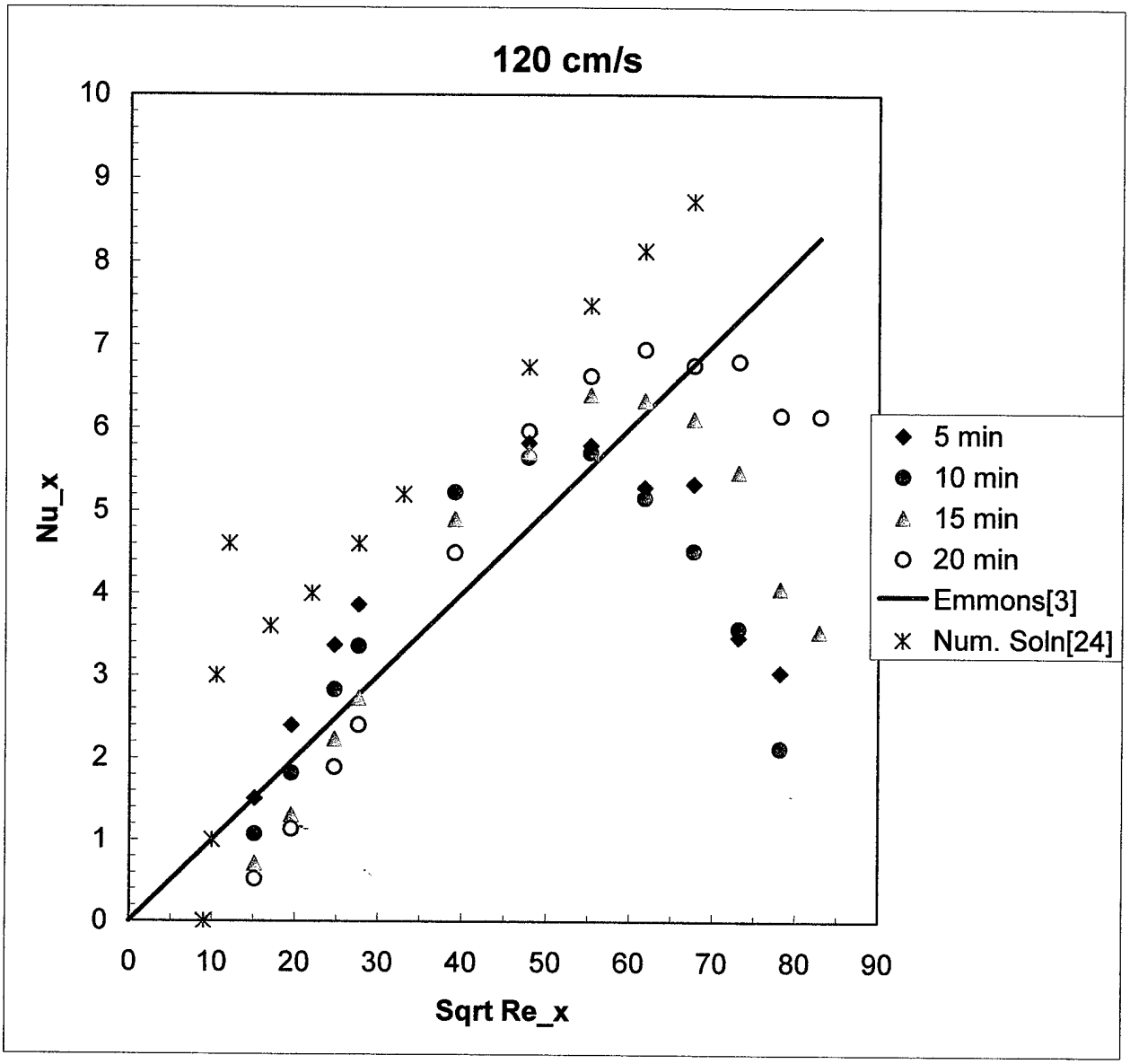

Figure 19: Normalized burning rate Nu_x versus $Re_x^{0.5}$ for U_∞ = 120 cm/s

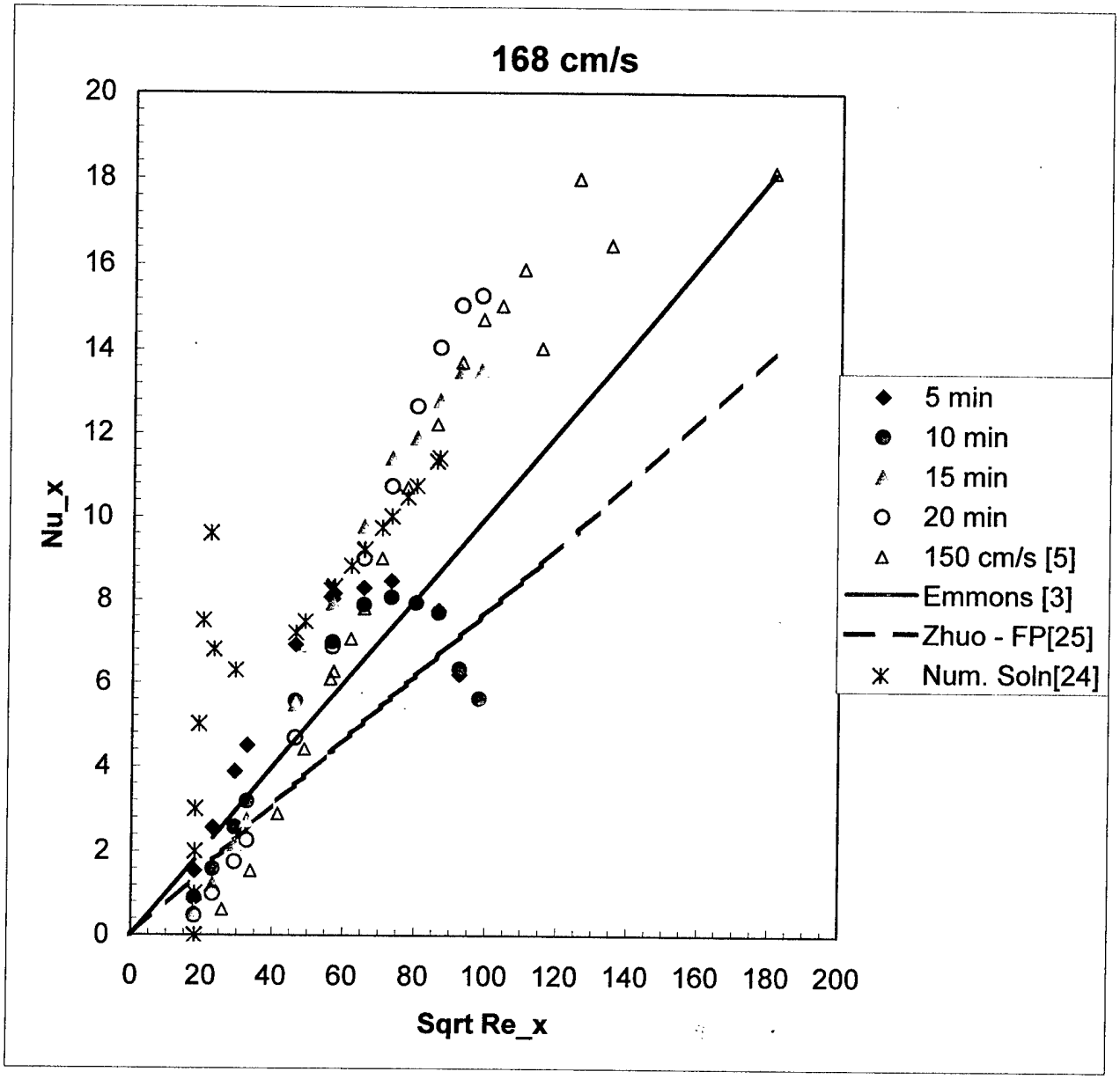

Figure 20: Normalized burning rate Nu_x versus $Re_x^{0.5}$ for U_∞ = 168 cm/s

Further tests were conducted where a large quenching distance was obtained in the leading section and the flame was slowly spreading upstream throughout the duration of the test. This was obtained by diluting the oxygen concentration in the incoming air with a flow of additional nitrogen to about 19.4% oxygen concentration (by volume). Details about these tests are in [26]. In these tests, because of the Damkohler number effects, the flame moved downstream after ignition, establishing about a 20 mm quenching distance. Thereafter, a small valley was established behind which the flame anchored and then spread very slowly upstream. With time, the valley deepened since the spread rate is very slow. Consequently, the surface regression decelerates in the leading section. Figure 21 shows a picture of the PMMA surface profiles after 5, 10 and 20-minute tests. It shows that the valley grew bigger with time just like in Fig. 11. Note that the flame had not spread up to the leading edge even in the 20 minutes test. Figure 22 shows the surface regression rate with X for these tests. It shows that the surface regression rate is transient in the leading section where the valley was formed, an indication that the presence of the valley is responsible for the transient behavior. Figure 22 shows that the peak regression rate decreased from a time-averaged value of 0.55 mm/min in 5 minutes to 0.32 mm/min in 20 minutes. Furthermore, in Fig. 22, the X distance where the regression rate is zero represents the location of the upstream edge of the valley. This can be used to approximate the leading edge of the flame. Thus, in 5, 10 and 20 minutes, the flame was about 11, 6 and 2 mm from the sample leading edge, respectively. One can therefore estimate that between 5 minutes and 10 minute after ignition, the time-averaged spread rate is about 1 mm/min; while between 10 minutes and 20 minutes, it is about 0.4 mm/min. Therefore, the spread rate decreases as the flame gets closer to the leading edge. These results indicate that in these slow spreading flames the regression rate in the leading section decreases with time and the spread rate upstream also decreases with time.

4.0 CONCLUSIONS

This report has presented a detailed experimental study of the burning characteristics of small PMMA samples under a forced flow boundary layer flame. The detailed characterization is necessary to provide a good understanding of the burning characteristics before a suppressing agent is added. The free stream velocity was varied between 60 and 168 cm/s. Gas phase temperature profiles were measured with fine thermocouples about 1 minute after a stable flame was established over the sample. Local time-averaged regression rates were measured along the length of the sample for tests lasting from 2.5 min to 20 minutes. The results can be summarized as follows: The peak gas phase temperature at each X location increased with stream-wise distance from the leading edge to a maximum (about 1900K at 84 cm/s) and then

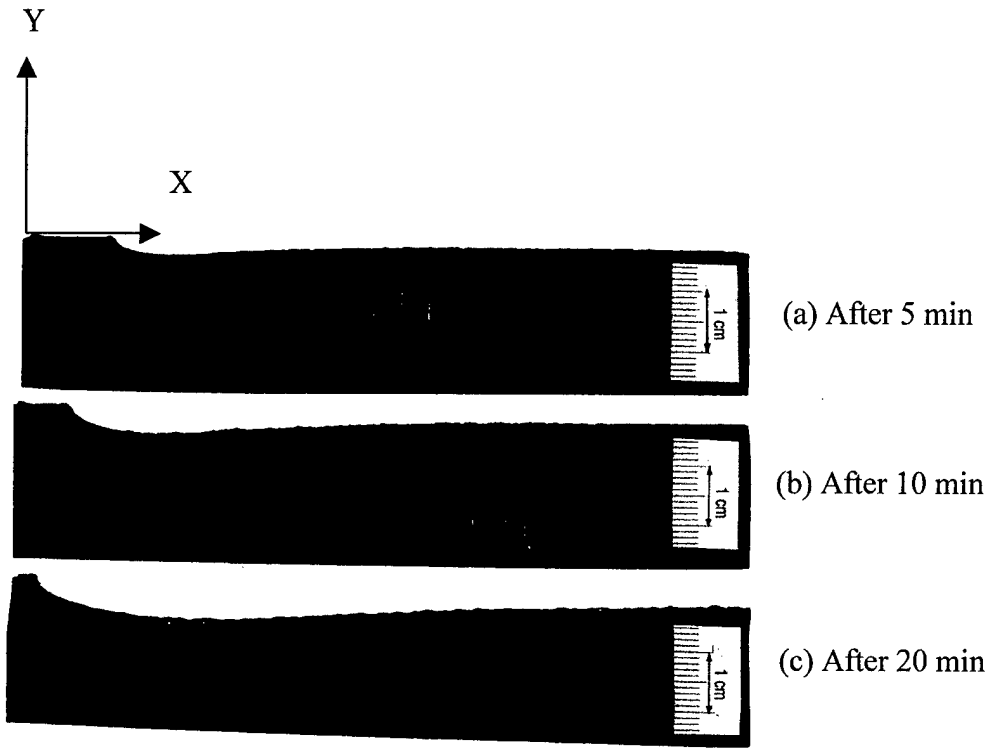

Figure 21 Sample surface profiles in 5, 10 and 20 minute tests , U_∞ = 84 cm/s, 19.4% oxygen. Flame creeping slowly upstream during the test

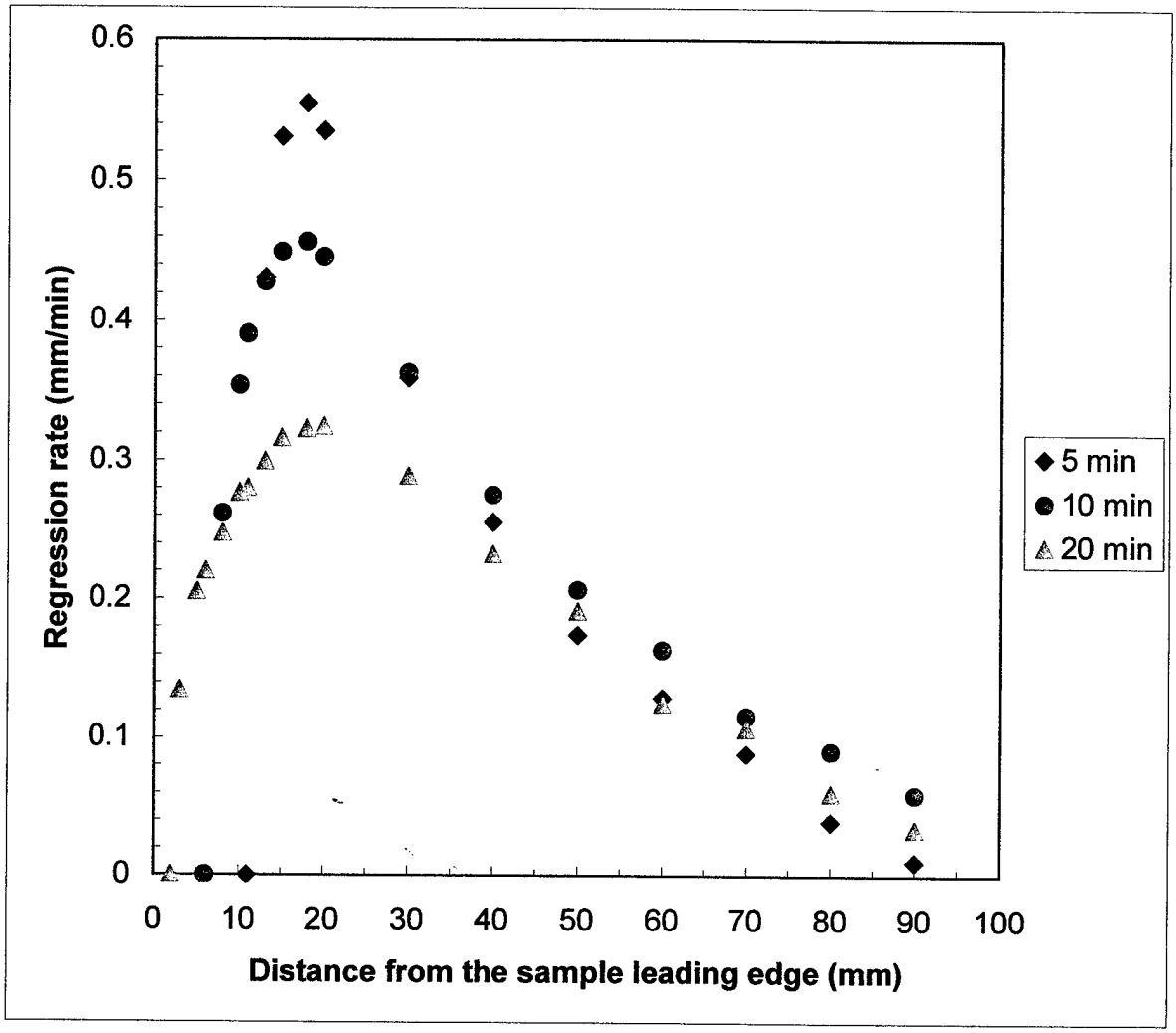

Figure 22: Regression rate with time at various X locations U_∞ = 84 cm/s, 19.4% oxygen flame slowly creeping upstream

- dropped as we get into the plume zone. The variation of flame standoff distance with Re_x is similar to the classical steady state prediction, an indication that a stable steady flame was obtain within a short time after ignition.
- The measured temperature in the PMMA molten layer ranges between 650K and 700K.
- The local burning rate is transient, decreasing with time near the leading edge (especially 10 mm $\leq$ X) and increasing with time downstream. The time averaged regression rate in the leading section decreased by about a factor of two between 5 and 20-minute tests within the inlet velocity range tested. The decrease in burning rate with time is due to the presence of a valley formed in the leading section as a result of non-uniform surface regression rate resulting from non-uniform heat feedback. It seems that as the valley increases with time the heat feedback to the surface in this section decreases because the flame standoff distance increases. The increase in regression rate with time in the trailing section seems to be due to in-depth solid conduction. In this section the heat feedback from the flame is very small; therefore, it takes considerable time (minutes) for the solid to warm up and start pyrolyzing at a significantly steady rate. A comparison of the normalized burning rate (in form of Nu_x) with the numerical predictions of Ananth et al. [24] reveal that at long times the measured data will approach the numerical predictions. At longer times the data could be higher than the steady state numerical predictions due to the moving boundary effects, which result in flame standoff distance decreasing with time.
- Finally, the results presented in this report show that transient burning rate due to non-uniform surface regression is obtainable when there is no upstream flame spread and when the flame is slowly creeping upstream.

5.0 ACKNOWLEDGEMENTS

We appreciate the contributions of Mr. Clarence Whitehurst in the experiments. This work was funded by the office of Naval Research, through Naval Research Laboratory and Code 334, under the Damage Control Task of the FY02 Surface Ship Hull, Mechanical and Electrical Technology Program

6.0 REFERENCES

1. Arisawa H and Brill T.B "Kinetics and mechanisms of flash pyrolysis of Poly(methyl methacrylate) (PMMA)" *Combust. Flame* 109 p.415 (1997)
2. Krishnamurthy L. and Williams F.A "Laminar combustion of poly methylmethacrylate in O_2/N_2 mixtures" 14th *Symposium (International) on Combustion, The combustion Institute, pp.1151 (1974)*
3. Emmons H.R., Zeit. Fur Angew. Math. and Mech. 36:60 (1956)
4. Hirano T and Kinoshita M " Gas velocity and temperature profiles of a diffusion flame stabilized in the stream over liquid fuel" *Fifteenth Symposium (International) on Combustion, The combustion Institute,* pp 379-387 (1975)

5. Agrawal, S Determination of surface heat flux in the burning zone during wind-aided flame spread using burned PMMA samples" Short Communication. *Combust. Sci. and Tech* **91** pp.187-190 (1993)
6. Atreya A. and Mekki K "Heat transfer during wind-aided flame spread on a ceiling mounted sample" *Twenty-fourth Symposium (International) on Combustion, The combustion Institute,* pp 1677-1684 (1992)
7. Fernandez-Pello A.C and Hirano T, (1983) "Controlling mechanisms of flame spread" *Combust. Sci. Tech.* 32 p.1
8. Kashiwagi T, Omori A and Nanbu H "Effects of Melt viscosity and thermal stability on polymer gasification" *Combust. Flame* **81**: 188 (1990)
9. Kashiwagi T. and Ohlemiller T.J., "A study of oxygen effects on non-flaming transient gasification of PMMA and PE during thermal radiation" Proc. Comb. Inst. **19**:815 (1982)
10. Vovelle, C: Akrich R; Delfau J.L and Gresillaud S. "Influence of the thickness on the thermal degradation of PMMA" *Fire Safety Science: Proceedings of the first International Symposium,* Hemisphere. Washington D.C pp473 (1986)
11. Tewarson, A. and Pion R.F., "Flammability of plastics – I Burning intensity" *Combust. Flame* **26** :85 (1976)
12. The temperature Handbook, Vol. 29; Omega Engineering Inc. (1995) pp. Z159.
13. Ndubizu, C.C; Ananth,R.; Tatem, P.A; and Motevalli, V; "On Water mist fire suppression mechanisms in a gaseous diffusion flame" *Fires Safety J.* **31:3** p.253 (1998)
14. Holve D.J and Sawyer R.F "Diffusion controlled combustion of polymers" *Fifteenth Symposium (International) on Combustion, The combustion Institute,* pp 351-361 (1974)
15. Orloff L., de Ris, J and Markstein G.H; *Fifteenth Symposium (International) on Combustion, The combustion Institute, Pittsburgh* pp.183-192 (1975)
16. Glassman I,. *Combustion* Academic Press Inc. London (1987) pp.284.
17. Eckert E.R.G and Drake R.M *Analysis of heat and mass transfer* McGraw-Hill Book Co. New York 1972 p.780
18. Ndubizu C.C and Zinn B.T "Effects of Metallic Additives upon Soot Formation in Polymer Diffusion Flames". *Combust Flames*, **46:**301-314. (1982)
19. Beier R.A and Pagni P.J "Soot volume fraction profiles in Forced-combusting boundary layers" *J. Heat Transfer* **105** pp 159-164 (1983)
20. Tewarson, A "Generation of heat and chemical compounds in fires" In *SFPE Handbook of Fire protection Engineering.* DiNenno P.J et. al (Eds.). National Fire Protection Association, Quincy, MA (1995) p. 3-68
21. ibid p. 3-71
22. Ndubizu C ; Ananth R ; Tatem P A and Whitehurst C " Stability and Flame spread over PMMA within the quenching distance" NRL Memorandum Report NRL/MR/ 6180
23. Handbook of Applied Engineering Science. Bolz R.E and Tuve G.L (Eds.) CRC Press Cleveland OH. 1976 pp.177 & 193
24. Ananth R, Ndubizu C; Tatem P.A; Patnaik R and Kailasanath K "Flow past a burning solid surface" Proceedings of the Halon Options Technical Working Conference, Albuquerque N.M, April 30- May 2 2002
25. Zhuo L and Fernandez-Pello A.C "Turbulent burning of a flat fuel surface" *Fire Safety Science: Proceedings of the third International Symposium,* Hemisphere. Washington D.C pp. 414-424 (1990)

26. Ndubizu C; Ananth R and Tatem P.A "Experimental study of water mist suppression mechanisms in a forced flow boundary layer flame" Proceedings of the Halon Options Technical Working Conference, Albuquerque N.M, April 24- 26, 2001

APPENDIX

TABLES OF REGRESSION RATE DATA

Table A1: **Variation of regression rate (mm/min) with X at various test duration**
U_∞ = 60 cm/s

X (mm)	*2.5 min*	*2.5 min*	*5 min*	*7.5 min*	*10 min*	*15 min*	*20 min*
0	1.38	1.325132	0.724702	0.527505	0.382414	0.236575	0.201489
3	1.088571	1.059474	0.939122	0.770239	0.649135	0.458924	0.436179
5	0.767532	0.682105	0.833041	0.738872	0.655302	0.517014	0.466055
8	0.54	0.526184	0.687649	0.671714	0.612724	0.509638	0.469529
10	0.461299	0.444868	0.588903	0.572278	0.583948	0.492119	0.459702
20	0.254805	0.303553	0.35511	0.358438	0.362055	0.37449	0.370471
30	0.202208	0.228553	0.212351	0.255618	0.240294	0.265423	0.285509
40	0.182727	0.173289	0.145768	0.159696	0.172659	0.212141	0.228089
50	0.147662	0.172105	0.124326	0.11974	0.138401	0.119276	0.156328
60	0.119221	0.094737	0.124138	0.087202	0.100033	0.102678	0.119752
70	0.071299	0.067895	0.041379	0.067939	0.078793	0.093919	0.119007
80	0.068961	0.047763	0.01768	0.018872	0.021436	0.056246	0.092506
90	0	0	0.020502	0.019002	0.062055	0.047289	0.066799

Table A2: **Variation of regression rate (mm/min) with X at various test duration**
U_∞ = 84 cm/s

X (mm)	*2.5 min*	*5 min*	*5 min*	*7.5 min*	*10 min*	*15 min*	*20 min*
0	1.545	0.71671	1.013333	0.56687	0.329213	0.279102	0.159917
3	1.216923	0.991548	1.02902	0.812609	0.671705	0.460745	0.371455
5	0.796538	0.964452	0.899412	0.825913	0.708098	0.554918	0.455851
8	0.556923	0.823161	0.751176	0.759913	0.682721	0.561818	0.486595
10	0.453462	0.710903	0.639804	0.681261	0.661869	0.555838	0.491702
20	0.261538	0.441871	0.402549	0.408522	0.477344	0.451544	0.43681
30	0.198077	0.327677	0.278039	0.310826	0.330393	0.332136	0.366446
40	0.161923	0.261871	0.230784	0.205565	0.245213	0.249792	0.295091
50	0.103077	0.223161	0.157059	0.161478	0.179508	0.189792	0.237273
60	0.100769	0.184452	0.141569	0.093522	0.132295	0.135115	0.188826
70	0.065769	0.145742	0.080588	0.043826	0.099836	0.088193	0.156347
80	0.041538	0.114774	0.044902	0.013435	0.060492	0.073275	0.128975
90	0	0.079935	0.028431		0.04918	0.060197	0.098727

Table A3: **Variation of regression rate (mm/min) with X at various test duration**
U_∞ = 120 cm/s

X (mm)	*2.5 min*	*5 min*	*7.5 min*	*10 min*	*15 min*	*20 min*
0	1.269020	0.627857	0.495983	0.365863	0.182308	0.144831
3	1.322745	0.991558	0.83738	0.703094	0.464967	0.340016
5	1.321176	0.945974	0.851659	0.71658	0.513692	0.447848
8	1.189412	0.830649	0.80345	0.697231	0.54844	0.466645
10	1.084314	0.761494	0.754454	0.661857	0.535912	0.474411
20	0.748235	0.515065	0.528603	0.515081	0.481582	0.4431
30	0.635686	0.382792	0.381616	0.371238	0.374505	0.392102
40	0.552157	0.285584	0.278646	0.281336	0.314703	0.327007
50	0.480392	0.208442	0.224279	0.203257	0.249231	0.274328
60	0.393333	0.17513	0.158122	0.148436	0.20044	0.222341
70	0.269412	0.097792	0.11738	0.100651	0.153692	0.191921
80	0.152157	0.075	0.056332	0.052378	0.09989	0.151855
90	0.002745	0.015974	0.018865	0.005472	0.077407	0.13479

Table A4: **Variation of regression rate (mm/min) with X at various test durations**
U_∞ = 168 cm/s

X (mm)	*2.5 min*	*2.5 min*	*5 min*	*10 min*	*15 min*	*20 min*	*20 min*
0	0	0.211923	0.457955	0.245401	0.139582	0.106639	0.09645
3	0.949091	1.053077	1.010607	0.591555	0.390725	0.348477	0.3121
5	1.089351	1.243462	1.007157	0.624648	0.479538	0.402666	0.39305
8	1.074935	1.267308	0.956741	0.632995	0.530703	0.445331	0.43265
10	0.988442	1.210385	0.886581	0.627005	0.538154	0.465894	0.44565
20	0.701688	0.876923	0.681853	0.548052	0.53789	0.493758	0.4608
30	0.561818	0.674231	0.527923	0.458789	0.519099	0.503046	0.45145
40	0.497143	0.566923	0.40869	0.388576	0.48033	0.495745	0.4437
50	0.472208	0.490769	0.333738	0.318069	0.448549	0.480993	0.42325
60	0.382208	0.319615	0.260895	0.260524	0.39	0.459089	0.41595
70	0.30974	0.176923	0.218339	0.216825	0.359341	0.431076	0.39595
80	0.253636	0.096923	0.15278	0.156137	0.331714	0.405844	0.37095
90	0.241948	0.006538	0.055591	0.123142	0.295187	0.343013	0.33475